

1 Assessing the roles emission sources and atmospheric processes play in simulating
2 $\delta^{15}\text{N}$ of atmospheric NO_x and NO_3^- using CMAQ (version 5.2.1) and SMOKE
3 (version 4.6).

4
5 *Huan Fang[†] and Greg Michalski[‡]*

6
7 [†]Department of Earth, Atmospheric, and Planetary Sciences Purdue University, 550 Stadium Mall
8 Drive, West Lafayette, IN 47907, United States

9
10 [‡]Department of Chemistry, Purdue University, 560 Oval Drive, West Lafayette, IN 47907, United
11 States

12
13
14 Correspondence: Huan Fang, fang63@purdue.edu

15
16 Keywords: isotope, nitrogen, atmospheric NO_x , atmospheric nitrate, NO_x emission sources,
17 emission inventory, emission input dataset, atmospheric processes, disperse, mixing, transport,
18 chemical transport model, 3D CTM, NEI, SMOKE, CMAQ

19

1 Abstract

2 Nitrogen oxides ($\text{NO}_x = \text{nitric oxide (NO)} + \text{nitrogen dioxide (NO}_2\text{)}$) are important trace gases that
3 affect atmospheric chemistry, air quality, and climate. Contemporary development of NO_x
4 emissions inventories is limited by the understanding of the roles of vegetation (net NO_x source or
5 net sink), vehicle emissions from gasoline- and diesel-powered vehicles, the application of NO_x
6 emission control technologies, and accurate verification techniques. The nitrogen stable isotope
7 composition ($\delta^{15}\text{N}$) of NO_x is an effective tool to evaluate the accuracy of the NO_x emission
8 inventories, which are based on different assumptions. In this study, we traced the changes in $\delta^{15}\text{N}$
9 values of NO_x along the “journey” of atmospheric NO_x , driven by atmospheric processes after
10 different sources emit NO_x to the atmosphere. The ^{15}N was incorporated into the emission input
11 dataset, generated from the US EPA trace gas emission model SMOKE (Sparse Matrix Operator
12 Kernel Emissions). Then the ^{15}N incorporated emission input dataset was used to run CMAQ (the
13 Community Multiscale Air Quality Modeling System). By enhancing NO_x deposition, we
14 simulated the expected $\delta^{15}\text{N}$ of NO_3^- assuming no isotope fractionation during chemical
15 conversion or deposition. The simulated spatiotemporal patterns in NO_x isotopic composition for
16 both SMOKE outputs (simulation under “emission only” scenario) and CMAQ outputs
17 (simulations under “emission + transport + enhanced NO_x loss” scenario) were compared with
18 corresponding measurements in West Lafayette, Indiana, USA. The simulations under “emission
19 + transport + enhanced NO_x loss” scenario was also compared to $\delta^{15}\text{N}$ of NO_3^- in NADP (National
20 Atmospheric Deposition Program) sites. The results indicate the potential underestimation of
21 emissions from soil, livestock waste, off-road vehicles, and natural gas power plants and the
22 potential overestimation of emissions from on-road vehicles and coal-fired power plants, if only
23 considering the difference in NO_x isotopic composition for different emission sources. After
24 considering the mixing, dispersion, transport, and deposition of NO_x emission from different
25 sources, the estimation of atmospheric $\delta^{15}\text{N}(\text{NO}_x)$ shows better agreement (by $\sim 3\%$) with
26 observations.

27

1. Introduction

Nitrogen oxides ($\text{NO}_x = \text{NO} + \text{NO}_2$) are important trace gases that affect atmospheric chemistry, air quality, and climate. The main sources of tropospheric NO_x are anthropogenic emissions from vehicles, power plants, agriculture, livestock waste, as well as natural emissions from lightning and the by-product of nitrification and denitrification occurring in soil (Galloway, et al., 2004). The NO_x photochemical cycle generates OH and HO_2 radicals, organic peroxy radicals (RO_2), and ozone (O_3), which ultimately oxidize NO_x into NO_y ($\text{NO}_y = \text{NO}_x + \text{HONO} + \text{HNO}_3 + \text{HNO}_4 + \text{N}_2\text{O}_5 + \text{other N oxides}$). During the photochemical processes that converts NO_x to NO_y , ground-level concentrations of O_3 become elevated and secondary particles are generated (Pandis and Sienfeld, 2003). Secondary aerosols that are hazardous to human health (Lighty et al., 2000) and affect cloud physics, enhancing the reflection of solar radiation (Schwartz, 1996). Thus, the importance of NO_x in air quality, climate, and human and environmental health makes understanding the spatial and temporal variation in the sources of NO_x a vital scientific question.

Despite years of research, however, there are still several significant uncertainties in the NO_x budget. About 15-40% of global NO_x emissions, ranging from 4 to 15 Tg N yr⁻¹, is derived from global soil NO_x emissions yet evaluating and verifying emission rates using laboratory, field measurements, and satellite observations is still a challenge (Jaeglé et al., 2005; Yan et al., 2005; Stehfest and Bouwman, 2006; Vinken et al., 2014; Rasool et al., 2016). Soil NO_x emissions vary by different biome types, meteorological conditions, N fertilizer application, and soil physicochemical properties (Ludwig et al., 2001). Furthermore, the role of vegetation, acting as a net source of atmospheric NO_x when ambient NO_x concentration is below the “compensation point”, versus acting as a net sink of atmospheric NO_x when ambient NO_x concentrations are above it (Johansson, 1987; Thoene, Rennenberg & Weber, 1996; Slovik et al., 1996; Webber & Rennenberg, 1996). This significantly impacts the biotic NO_x emission inventory (Almaraz et al., 2018). Uncertainties also exist in the amount of NO_x emitted during the combustion of fossil fuels by vehicles and industry. According to Parrish (2006), the estimation of on-road vehicle NO_x emission has at least 10 to 15% uncertainty. For the mileage-based algorithm, which is used in the National Emission Inventory (NEI), the uncertainty is caused by the limited number of sites to determine the emission factors of vehicle classifications and emission types (Ingalls, 1989; Pierson et al., 1990; Fujita et al., 1992; Pierson et al., 1996; Singer and Harley, 1996). The uncertainty in power plant NO_x emissions results from the choice of emission control technologies, of which the removal efficiencies of NO_x emission are different. NO_x removal by low NO_x burning, over-fire air reduction, and selective non-catalytic reduction is highly variable, ranging from 50 to 75% (Srivastava et al., 2005).

The nitrogen stable isotope composition of NO_x might be a useful tool to help resolve the uncertainties of how NO_x emission sources vary in space and time because NO_x sources have distinctive ¹⁵N/¹⁴N ratios (Ammann et al., 1999; Felix et al., 2012; Felix and Elliott, 2013; Fibiger et al., 2014; Heaton, 1987; Hoering, 1957; Miller et al., 2017; Walters et al., 2015a, 2015b, 2018). This variability in NO_x ¹⁵N/¹⁴N ratios is quantified by

$$\delta^{15}\text{NO}_x (\text{‰}) = [({}^{15}\text{NO}_x/{}^{14}\text{NO}_x) / ({}^{15}\text{N}_2/{}^{14}\text{N}_2)_{\text{air}} - 1] \times 1000 \quad \text{Eq. (1)}$$

where ¹⁵NO_x/¹⁴NO_x is the measurement of ¹⁵N/¹⁴N in atmospheric NO_x , compared with the ratios in air $\text{N}_2 = 0.0036$ (For brevity, the $\delta^{15}\text{N}$ value of any NO_y compound will be denoted as $\delta^{15}\text{NO}_y$; e.g. $\delta^{15}\text{NO}_3^-$). Previous research has shown that there are unique differences in $\delta^{15}\text{N}$ values for

1 NO_x from different emission sources and significant
 2 variations within each source (Fig. 1). This
 3 uniqueness can potentially be used to partition the
 4 relative importance of various NO_x sources in a
 5 mixed atmosphere. For example, Redling et al.
 6 (2003) found higher δ¹⁵N of NO₂ in samples
 7 collected closer to the highway compared to those
 8 adjacent to a forest, showing the emissions from
 9 vehicles were dominant near the highway. A strong
 10 positive correlation between δ¹⁵NO₃⁻ and NO_x
 11 emission from coal-fired power plants within 400
 12 km radial area of study sites of deposition suggest
 13 local power plant NO_x emissions impacted regional
 14 NO_x budgets (Elliott et al., 2007; 2009). What is
 15 lacking is a systematic way of evaluating δ¹⁵NO_y
 16 values in numerous studies in the context of NO_x
 17 sources, regional emissions, meteorology, and
 18 atmospheric chemistry (Elliott et al., 2009; Garten, 1992; Hall et al., 2016; Occhipinti, 2008;
 19 Russell et al., 1998).

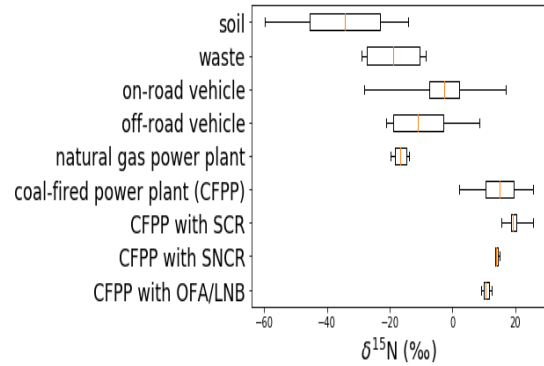


Figure 1: Box (lower quartile, median, upper quartile) and whisker (lower extreme, upper extreme) plot of the distribution of δ¹⁵N values for various NO_x emission sources.

20 Here we have simulated the emission of ¹⁵NO_x and its mixing in the atmosphere and compared
 21 the predicted δ¹⁵N (NO_x, NO₃⁻) values to observations. The δ¹⁵NO_x values are impacted by three
 22 main factors. The first is the inherent variability of the δ¹⁵NO_x emissions in time and space.
 23 Secondly, atmospheric processes that mix the emitted NO_x, dispersing multiple emission sources
 24 within a mixing lifetime relative to the NO_x chemical lifetime (2-7 hours), which depends on its
 25 concentration and photooxidation chemistry, that also vary in time and by location (Laughner &
 26 Cohen, 2019). And thirdly, isotope effects occurring during tropospheric photochemistry may alter
 27 the δ¹⁵NO_x emissions as they are transformed from NO_x into NO_y. In this paper, we consider the
 28 effects from the first and second considerations, the temporal and spatial variation in NO_x emission
 29 and the impacts from atmospheric transport and deposition processes (source and mixing
 30 hypothesis). We accomplish this by incorporating an input dataset of ¹⁵N emissions used in
 31 simulations by the CMAQ (Community Multiscale Air Quality) modeling system. In a previous
 32 paper we have discuss the impacts of tropospheric photochemistry by incorporating a ¹⁵N chemical
 33 mechanism (Fang et al., 2021) into CMAQ. The ultimate goal is to evaluate the accuracy of the
 34 NO_x emission inventory using ¹⁵N.

35 2. Methodology

36 2.1 Incorporating ¹⁵N into NO_x emission datasets

37 The EPA trace pollutant emission model SMOKE (Sparse Matrix Operator Kernel Emissions)
 38 was used to simulate ¹⁴NO_x and ¹⁵NO_x emissions. ¹⁴NO_x emissions were estimated using the
 39 SMOKE model based on the 2002 NEI (National Emission Inventory, USEPA, 2014), and ¹⁵N
 40 emissions were determined using these ¹⁴NO_x emissions and the corresponding δ¹⁵N values of NO_x
 41 sources from previous research (Table 1). Using the definition of δ¹⁵N (‰), ¹⁵NO_x emitted by each
 42 SMOKE processing category (area, biogenic, mobile, and point) was calculated by

$$43 \quad {}^{15}\text{NO}_x(i) = {}^{14}\text{NO}_x(i) \times {}^{15}\text{R}_{\text{NO}_x}(i) \quad \text{Eq. (2)}$$

44 where ¹⁴NO_x(i) are the NO_x emissions for each category (i) obtained from NEI and SMOKE and
 45 ¹⁵R_{NO_x} is a ¹⁵N emission factor (¹⁵NO_x_i/¹⁴NO_x_i) calculated by rearranging Eq. 1:

$${}^{15}R_{NO_x}(i) = \left(\frac{\delta^{15}NO_x(i)}{1000} + 1 \right) \times 0.0036 \quad \text{Eq. (3)}$$

$\delta^{15}NO_x(i)$ is the $\delta^{15}N$ value of some NO_x source ($i = \text{area, biogenic, mobile, and point}$).

Annual NO_x emissions for 2002 were obtained from the NEI at the county-level and were converted into hourly emissions on a 12 km x 12 km grid as previously published (Spak, Holloway, & Stone, 2007). The modeling domain includes latitudes between 37 ° N and 45 ° N, and longitudes between 98° W and 78° W, which fully covers the Midwestern US (Fig. 2, in yellow). SMOKE categorizes NO_x emissions into four “processing categories”: Biogenic, Mobile, Point, and Area (Table 1). The choice of the 2002 version of NEI is, in part, arbitrary. However, to compare the model predicted $\delta^{15}N$ values with observations, it requires the emission inventory to be relevant to the same timeframe as the $\delta^{15}N$ measurements of the NO_y . The data sets we compare to the model (discussed below) span from 2002 to 2009, thus the 2002 inventory is more relevant than later inventories (2014 onward). The county-level annual ${}^{14}NO_x$ emission for the Midwestern US from NEI was converted to the dataset with hourly ${}^{14}NO_x$ emissions.

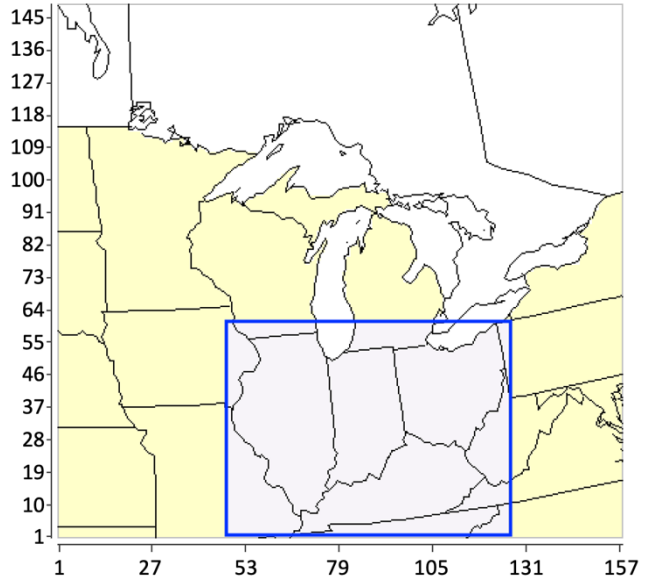


Figure 2: The full geographic domain (yellow) and extracted domain (light grayish purple) for the study.

SMOKE Category	NEI Sector	$\delta^{15}N\text{-}NO_x$ (‰) range	$\delta^{15}N\text{-}NO_x$ (‰) this study
Biogenic	Soil	-59.8 ~ -14.0	-34.3 (Felix & Elliott, 2014)
Area	Livestock Waste	-29 ~ -8.5	-18.8 (Felix & Elliott, 2014)
	Off-road Gasoline	-21.1 ~ 8.5	-11.5 (Walters et al., 2015b)
	Off-road Diesel		-10.5 (Walters et al., 2015b)
Mobile	On-road Gasoline	-28.1 ~ 17	-2.7 (Walters et al., 2015b)
	On-road Diesel		-2.5 (Walters et al., 2015b)
Point	Coal-fired Fossil Fuel Combustion	-19.7 ~ 25.6	15 (Felix et al., 2012)
	Natural Gas Fossil Fuel Combustion		-16.5 (Walters et al., 2015)

Table 1: The $\delta^{15}N$ values (in ‰) for NO_x emission sources based on SMOKE processing category and NEI sector

2.1.1 Biogenic ${}^{15}NO_x$ emissions

The NO_x emission from the soil (Biogenic) was modeled in SMOKE using standard techniques (details in SA) and the $\delta^{15}N$ values of biogenic NO_x were taken from previous studies.

1 Li & Wang (2008) measured the NO fluxes using dynamic flow chambers for 2 to 13 days after
 2 cropland soil was fertilized by either urea (n=9) or ammonium bicarbonate (n=9), and the $\delta^{15}\text{NO}_x$
 3 ranged from -48.9‰ to -19.8‰. Felix & Elliott (2014) used passive samplers to collect NO_2 in a
 4 cornfield for 20 days, with low (-30.8‰) and high (-26.5‰) fertilizer application. Using active
 5 samplers, Miller et al. (2018) collected NO_2 between May and June finding $\delta^{15}\text{N}$ ranging from -
 6 44.2‰ to -14.0‰ (n=37); Yu & Elliott (2017) measured -59.8‰ to -23.4‰ in 15 samples from
 7 soil plots in a fallow field 2 weeks after the precipitation. Based on these studies we adopted an
 8 average $\delta^{15}\text{N}$ value for NO_x emissions from the soil of -34.3‰ (Li & Wang, 2008; Felix & Elliott,
 9 2014; Yu & Elliott, 2017; Miller et al., 2018).

11 2.1.2 Mobile $^{15}\text{NO}_x$ emissions

12 The SMOKE NO_x emission from on-road vehicles used standard methods (details in SA) and
 13 used $\delta^{15}\text{N}$ values from prior studies. We have excluded studies that infer $\delta^{15}\text{N}$ NO_x by measuring
 14 plant proxies or passive sampling in the environment (Ammann et al., 1999; Pearson et al., 2000;
 15 Savard et al. 2009; Redling et al., 2013; Felix & Elliott, 2014). This is because equilibrium and
 16 kinetic isotope effects occur as NO_x reacts in the atmosphere to form NO_y , prior to NO_x deposition.
 17 In addition, the role vegetation plays in NO_x removal and atmospheric processes that mix emitted
 18 NO_x with the surroundings can also alter the $\delta^{15}\text{NO}_x$. Instead, we estimated the $\delta^{15}\text{NO}_x$ emissions
 19 from vehicles only using studies that directly measured tailpipe NO_x emissions. Moore (1977) and
 20 Heaton (1990) collected tailpipe NO_x spanning -13‰ to 2‰, with an average of -7.5 ± 4.7 ‰.
 21 Neither Heaton nor Moore noted whether these 6 vehicles were equipped with any catalytic NO_x
 22 reduction technology, but it is unlikely since the late 1970 and 80's vehicles were seldomly
 23 equipped with catalytic NO_x reduction technology. Fibiger (2014) measured 5 samples of NO_x
 24 from diesel engines without SCR emitted into a smog chamber, the $\delta^{15}\text{N}$ values range from -19.2‰
 25 to -16.7‰ (± 0.97 ‰). The most comprehensive studies on vehicle NO_x $\delta^{15}\text{N}$ values are by Walters
 26 et al. (2015a, 2015b) who measured gas and diesel vehicles separately, including those with and
 27 without three-way catalytic converter (TCC) and SCR technology. They also measured on-road
 28 and off-road vehicles separately. The measurements showed that the $\delta^{15}\text{NO}_x$ emitted by on-road
 29 diesel vehicles ranged from -5‰ to 0‰, so the average -2.5‰ was adopted. The $\delta^{15}\text{NO}_x$ values
 30 emitted by on-road gasoline vehicles is a function of vehicle travel times, ranged from -6.3‰ to
 31 1.8‰ with the average -2.7 ± 0.8 ‰ for the Midwest region. This value is close to the measurements
 32 (-8‰ to -1‰, averaged -4.7 ± 1.7 ‰) of Miller et al. (2017) who collected NO_x along highways in
 33 Pennsylvania and Ohio.

34 The emission rate of $^{15}\text{NO}_x$ from the mobile source was determined by Eq. 4 grid by grid,
 35 according to the contributions from on-road gasoline vehicles and on-road diesel vehicles, as well
 36 as their corresponding $\delta^{15}\text{N}$ values. NO_x emissions from off-road vehicles are regarded as area
 37 sources in SMOKE, which were processed over each county. In contrast, NO_x emissions from on-
 38 road vehicles are regarded as the mobile source in SMOKE, which will be processed along each
 39 highway. The $\delta^{15}\text{N}$ of on-road gasoline vehicles was based on the average of the vehicle travel
 40 time (t) within each region with the same zip code (Walters et al., 2015b).

$$41 \quad {}^{15}\text{NO}_x (\text{mobile}) = \left(\frac{\delta^{15}\text{NO}_x (\text{on-road gas})}{1000} + 1 \right) \times 0.0036 \times {}^{14}\text{NO}_x (\text{on-road gas})$$

$$42 \quad + \left(\frac{\delta^{15}\text{NO}_x (\text{on-road diesel})}{1000} + 1 \right) \times 0.0036 \times {}^{14}\text{NO}_x (\text{on-road diesel}) \quad \text{Eq. (4)}$$

$$43 \quad \text{Where } \delta^{15}\text{NO}_x (\text{on-road gas}) = -12.35 + 3.02 \times \ln(t + 0.455)$$

45 2.1.3 Point source $^{15}\text{NO}_x$ emissions

1 NO_x point sources are large anthropogenic NO_x emitters located at a fixed position such as
2 EGUs (electric generating units). Fugitive dust does not significantly contribute to point NO_x
3 emissions, so our inventory focused only on power plants (Houyoux, 2005). Power plants were
4 separated into two different types: EGU and Non-EGU (e.g. commercial and industrial
5 combustions). The δ¹⁵N value of NO_x emitted from power plants have been estimated to vary from
6 -19.7‰ to 25.6‰ (Heaton, 1987; Heaton, 1990; Snape, 2003; Felix et al., 2012; Walters et al.,
7 2015b). We have ignored studies that measured δ¹⁵NO₃⁻ or δ¹⁵HNO₃ from EGUs (Felix et al., 2015,
8 Savard et al., 2017) and instead, only consider those studies that directly measured δ¹⁵NO_x from
9 stacks. Heaton (1990) collected 5 samples from the different coal-fired power stations finding NO_x
10 from 6‰ to 13‰, with a standard deviation of 2.9‰. Snape (2003) measured δ¹⁵N values from
11 power plants using three different types of coals values ranging from 2.1‰ to 7.2‰, with a
12 standard deviation of 1.37‰ (n= 36). The most comprehensive study on coal-fired power plants
13 NO_x values was by Felix et al. (2012). They measured the δ¹⁵NO_x emission from the coal-fired
14 power stations with and without different emission control technologies. The δ¹⁵NO_x emissions
15 range from 9‰ to 25.6‰, with the average 14.2±4.51‰ (n=42). The δ¹⁵NO_x values varied when
16 different emission control technologies were used: ranging from 15.5‰ to 25.6‰ with the average
17 19.4±2.28‰ (n=16) for SCR; ranging from 13.6‰ to 15.1‰ with the average 14.2±0.79‰ (n=3)
18 for SNCR; range from 9.0‰ to 12.6‰ with the average 10.7±1.11‰ (n=15) for OFA/LNB; range
19 from 9.6‰ to 11.7‰ with the average 10.5±0.79‰ (n=8) for no emission control technology.
20 According to Xing et al. (2013), about half of the coal-fired power plants in the United States are
21 equipped with SCR. Thus, we assume 15‰ for the NO_x emissions from coal-fired power plants,
22 which is the average between SCR and other emission control technologies.

23 The most comprehensive study on natural gas-fired δ¹⁵NO_x values (Walters et al. 2015)
24 collected NO_x from a residential a natural gas low-NO_x furnace and the stack of a natural gas EGU.
25 The measurement showed that the δ¹⁵N values of NO_x emitted by natural gas power plants ranged
26 that average -16.5±1.7‰, which we used for the NO_x emission from natural gas power plants. The
27 latitude, longitude, and point sources characteristics (EGU and non-EGU, coal-fired or natural gas-
28 fired, implementation of emission control technology) of each power plant was obtained from the
29 US Energy Information Administration (2017). The power plants were assigned grids by their
30 latitudes and longitudes, and the δ¹⁵N values were assigned to these grids based on their emission
31 characteristics, before determining the emission rate of ¹⁵NO_x from point source using Eq. (2) and
32 (3).

34 2.1.4 Area source ¹⁵NO_x emissions

35 Area NO_x (details in SA) δ¹⁵N values were based on the assumption that livestock waste and
36 off-road vehicles (utility vehicles for agricultural and residential purposes) accounted for total area
37 sources. Livestock waste δ¹⁵NO_x values were taken from Felix & Elliott (2014) since it is currently
38 the only study livestock waste emissions. They placed a passive sampler with ventilation fans in
39 an open-air and closed room in barns of cows and turkeys, respectively. The δ¹⁵NO_x emissions
40 from these measurements range from -29‰ to -8.5‰. Among these samples, the δ¹⁵NO_x emissions
41 from turkey waste averaged -8.5‰, the δ¹⁵NO_x emissions from cow waste averaged -24.7‰. We
42 used -18.8‰ as the values of δ¹⁵NO_x emissions from livestock waste, which is the weighted
43 average of the from turkey waste and cow waste emissions. We used Walters et al. (2015b) to
44 estimate the δ¹⁵NO_x emissions from the off-road vehicles since it is the latest in-depth study that
45 measured the δ¹⁵NO_x specifically from off-road vehicles that ranged from -15.6‰ to -6.2‰,
46 averaged -11.5±2.7‰. The measurement showed that the δ¹⁵N values of NO_x emitted by diesel

1 off-road vehicles without SCR ranged from -21.1‰ to -16.8‰, averaged -19‰±2‰, and diesel-
 2 powered off-road vehicles with SCR ranged from -9‰ to 8.5‰, averaged -2‰±8‰. We adopted
 3 -10.5‰ for $\delta^{15}\text{N}$ values of NO_x emitted by diesel-powered off-road vehicle, which is the median
 4 between the measurement of vehicles with and without SCR.

5 The emission rate of $^{15}\text{NO}_x$ from area source was determined by Eq. 5 grid by grid, according
 6 to the contributions from waste, off-road gasoline vehicle, and off-road diesel vehicle, as well as
 7 their corresponding $\delta^{15}\text{N}$ values based on previous research.

$$\begin{aligned}
 8 \quad ^{15}\text{NO}_x(\text{area}) &= \left(\frac{\delta^{15}\text{NO}_x(\text{waste})}{1000} + 1 \right) \times 0.0036 \times ^{14}\text{NO}_x(\text{waste}) \\
 9 \quad &+ \left(\frac{\delta^{15}\text{NO}_x(\text{off-road gas})}{1000} + 1 \right) \times 0.0036 \times ^{14}\text{NO}_x(\text{off-road gas}) \\
 10 \quad &+ \left(\frac{\delta^{15}\text{NO}_x(\text{off-road diesel})}{1000} + 1 \right) \times 0.0036 \times ^{14}\text{NO}_x(\text{off-road diesel}) \quad \text{Eq. (5)}
 \end{aligned}$$

11
 12
 13 The $^{15}\text{NO}_x$ emission data files of each SMOKE processing category were incorporated into the
 14 final dataset based on the $\delta^{15}\text{N}$ values from previous research (Table 1) and Eq. (2-5).
 15

$$\delta^{15}\text{NO}_x(\text{total}) = \left(\frac{^{15}\text{NO}_x(\text{area}) + ^{15}\text{NO}_x(\text{biog}) + ^{15}\text{NO}_x(\text{mobile}) + ^{15}\text{NO}_x(\text{point})}{^{14}\text{NO}_x(\text{area}) + ^{14}\text{NO}_x(\text{biog}) + ^{14}\text{NO}_x(\text{mobile}) + ^{14}\text{NO}_x(\text{point})} - 1 \right) \times 1000 \quad \text{Eq. (6)}$$

19 2.2 Simulating atmospheric $\delta^{15}\text{NO}_x$ in CMAQ

20 In order to investigate the role of mixing in the spatiotemporal distribution of $\delta^{15}\text{NO}_x$ values,
 21 CMAQ was used to simulate the meteorological transport effects (advection, eddy diffusion, etc.).
 22 In this “emission + transport” scenario, grid specific $\delta^{15}\text{NO}_x$ values emitted are dispersed as NO_x
 23 mixes across the regional scale. This dispersion will depend on grid emission strength and mixing
 24 vigor and is effectively treating NO_x as a conservative tracer. The simulations used the 2002
 25 National Emission Inventory (NEI), as well as 2002 and 2016 meteorological conditions
 26 respectively, to explore how meteorological conditions will impact the atmospheric $\delta^{15}\text{NO}_x$.
 27 Simulations covering the full domain and extracted domain were conducted to explore and
 28 eliminate potential bias near the domain boundary.
 29

30 2.2.1 Meteorology input dataset and boundary conditions

31 To explore the impact of atmospheric processes, the meteorology input datasets for the years
 32 2002 and 2016 were prepared and compared. The CMAQ CTM (CCTM) used the NARR (North
 33 American Regional Reanalysis) and NAM (North American Mesoscale Forecast System) to
 34 convert the weather observations (every 3 hours for NARR, every 6 hours for NAM Analyses)
 35 into gridded meteorological elements, such as temperature, wind field, and precipitation, with the
 36 horizontal resolution of 12 km, and 34 vertical layers, with the thickness, increases with height,
 37 from 50 m near the surface to 600 m near the 50 mb pressure level. These were used to generate
 38 the gridded meteorology files on an hourly basis, using the Weather Research and Forecasting
 39 Model (WRF). To maintain consistency between the NO_x emission dataset and the meteorology,
 40 the same coordinate system, spatial domain, and grid size used in the SMOKE model were used
 41 in the WRF simulation. The WRF outputs were used to prepare the CMAQ-ready meteorology
 42 input dataset using CMAQ’s MCIP (the Meteorology-Chemistry Interface Processor; see SA for

1 details). In these emission-only simulations, the deposition of NO_x was effectively set to zero. This
2 was accomplished by defining $\text{YO} = {}^{14}\text{NO}$ and $\text{YO}_2 = {}^{14}\text{NO}_2$ (in addition to $\text{ZO} = {}^{15}\text{NO}$ and $\text{ZO}_2 =$
3 ${}^{15}\text{NO}_2$) and setting their deposition velocities to 0.001 (setting them to zero collapses the
4 simulation). The meteorological fields generated by MCIP were used as the inputs for Initial
5 Conditions Processor (ICON) and Boundary Conditions Processor (BCON) to run CCTM in
6 CMAQ. The ICON program prepares the initial chemical/isotopic concentrations in each of the
7 3D grid cells for use in the initial time step of the CCTM simulation. The BCON program prepares
8 the chemical/isotopic boundary condition throughout the CCTM simulation. The CMAQ default
9 ICON and BCON for a clean atmosphere were used, which had $\text{NO}_x < 0.25$ ppb. The ${}^{15}\text{NO}_x$ were
10 added to the outputs of ICON and BCON, with the concentration equal to $0.0036[{}^{14}\text{NO}_x]$, which
11 assumes $\delta^{15}\text{N} = 0$ at the initial time step and outside the domain of the simulation.

12 13 2.2.2 The role of deposition and chemical transformation of NO_x

14 CMAQ simulated how NO_x removal by photochemical oxidation and deposition alters
15 $\delta^{15}\text{NO}_x$ during mixing, transport, and dispersion. This “apparent” conversion of NO_x to NO_y was
16 implemented by enhancing NO_x dry deposition by first magnifying it to 20 times normal (14
17 kg/hectare/yr) and testing for the change in NO_x concentration relative to the normal deposition
18 rate. Multiple tuning trials were conducted until the e-folding time (lifetime) of NO_x in the
19 atmosphere across the domain averaged about 1 day. This is a typical average photochemical NO_x
20 lifetime for a combination of urban, suburban, and rural environments (Laughner & Cohen, 2019).
21 This approach is limited since NO_x lifetime varies depending on oxidation capacity, with urban
22 NO_x lifetimes (~2-11 hours) being significantly shorter than in rural conditions (Fang et al., 2021).
23 In these simulations, the molecular mass of Y and Z were set equal (14) to ensure no isotope effect
24 was induced by dry deposition, since the equations for dry deposition have a mass term in the
25 diffusion coefficient calculation. These “emission + transport + enhanced NO_x loss” simulations
26 are an attempt to show how “lifetime chemistry” alters $\delta^{15}\text{NO}_x$ values by removing NO_x before it
27 can be transported along significant distances. For example, in an “emission + transport” scenario
28 NO_x from a high emission powerplant could travel across the domain altering regional $\delta^{15}\text{NO}_x$ as
29 it mixes with other grids. In contrast, in the “emission + transport + enhanced NO_x loss” scenario
30 most of that NO_x would be removed near the power plant, effectively constricting its $\delta^{15}\text{N}$
31 influence. This has an added advantage in that the deposited $\delta^{15}\text{NO}_x$ should be similar to the
32 $\delta^{15}\text{NO}_3^-$, which is not being generated in this model. We emphasize that in this model the isotope
33 effects associated with the photochemical transformation of NO_x into HNO_3 (and other higher N
34 oxides) and deposition are ignored and will be addressed in a forthcoming paper.

35 36 2.2.4 The simulation over the extracted domain

37 As mentioned in section 2.2.1, atmospheric $\delta^{15}\text{NO}_x = 0\text{‰}$ for initial condition and boundary
38 condition. As a result, a bias may occur along the boundary of the research area and mainly occurs
39 under the following two circumstances. Firstly, when the air mass transports out of the research
40 area (Fig. S1). Due to the lack of the emission dataset, Canada is considered an “emission-free
41 zone” for this research. As a result, the atmospheric NO_x is diluted, which impacts its $\delta^{15}\text{N}$ values,
42 especially for those with extreme $\delta^{15}\text{N}$ values ($\delta^{15}\text{N} < -15\text{‰}$ or $\delta^{15}\text{N} > 5\text{‰}$). Secondly, the air mass
43 with $\delta^{15}\text{NO}_x = 0$ transports from the “emission-free zone” into the research area (Fig. S2), the
44 atmospheric $\delta^{15}\text{NO}_x$ is flattened. Therefore, to avoid the bias near the border, the extracted domain
45 that only covers Indiana, Illinois, Ohio, and Kentucky was determined (Fig. 2, in light purple),
46 where the measurements of $\delta^{15}\text{N}$ values at NADP sites are available (Mase, 2010; Riha, 2013).

1 The boundary condition for the simulation over the extracted domain is based on the CCTM output
2 of the full-domain simulation (BCON code available on Zenodo.org (10.5281/zenodo.4311986)).
3

4 3. Results and Discussion

5 3.1 Simulated spatial variability of NO_x emission rates

6 We first examine the spatial
7 heterogeneity of the NO_x emission rate for a
8 single time period to illustrate the overall
9 pattern of NO_x emission over the domain
10 (Fig. 3). This is because the $\delta^{15}\text{NO}_x$ emission
11 is determined by the fraction of each NO_x
12 source (Eq. 6), which in turn is a function of
13 their emission rates. Since our NO_x emissions
14 are gridded by SMOKE using the NEI, they
15 are, by definition, correct with respect to the
16 NEI. However, a brief discussion of the
17 salient geographic distribution of NO_x
18 emissions and comparisons with other studies
19 is warranted for completeness and as a
20 backdrop for the discussion of NO_x fractions
21 and resulting $\delta^{15}\text{N}$ values. We have arbitrarily
22 chosen to sum the NO_x emissions during the
23 April to June time period for this discussion
24 (Fig. 3).

25 The April to June NO_x emissions ranged
26 from less than 0.01 tons N/day to more than
27 15 tons N/day, with the seasonal grid average of 0.904 tons N/day. This average agrees well with
28 estimates in previous studies for the United States, which were between 0.81 and 1.02 tons N/day
29 (Dignon & Hameed, 1989; Farrell et al., 1999; Selden et al., 1999; Xing et al, 2012). Within 75%
30 of the geographic domain, the NO_x emissions are relatively low, ranging from between 0 and 0.5
31 tons N/day (Fig. S3). Geographically, these grids are in rural areas some distance away from
32 metropolitan areas and highways (Fig. 3). NO_x emissions within about 20% of the grids is
33 relatively moderate, ranging between 0.5 and 2.0 tons N/day (Fig. S3). Geographically, these grids
34 are mainly located along major highways and areas with medium population densities (Fig. 3).
35 Urban centers comprise about 5% of the grids within the geographic domain and these have high
36 NO_x emissions rates, ranging between 2.0 and 15.0 tons N/day (Fig. S3). The metropolitan area's
37 average is 5.03 tons N/day, which is nearly 14 times of the average emission rate over the rest of
38 the grids within the geographic domain (0.37 tons N/day) due to the high vehicle density associated
39 with high population. The highest emissions rates are located within large cities as well as the edge
40 of the east coast metropolitan area (Fig. 3). Summing the NO_x emissions among the grids that
41 encompass these major midwestern cities, yields city-level NO_x emission rates that vary from 61.2
42 tons N/day (Louisville, KY) to 634.1 tons N/day (Chicago, IL). These city-level NO_x emission
43 rates (Table S4) agree well with estimates derived from the Ozone Monitoring Instrument (Lu et
44 al., 2015). Grids containing power plants are the significant NO_x hotspots within the geographic
45 domain. These account for less than 1% of the grids, but the NO_x emissions from a single grid that
46 contains a power plant can be as high as 93.4 tons N/day. Geographically, the power plants are

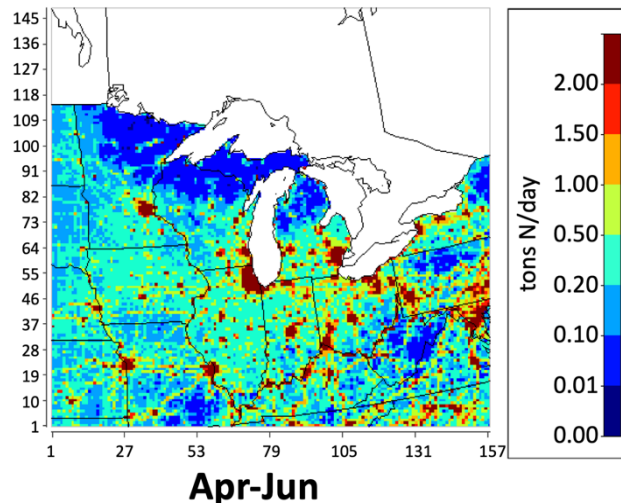


Figure 3: Total NO_x emission in the Midwest between April and June in tons N/day. High NO_x emissions are associated with major urban areas such as Chicago, Detroit, Minneapolis-St Paul, Kansas City, St. Louis, Indianapolis, and Louisville.

1 mainly located along the Ohio River valley, near other water bodies, and often close to
 2 metropolitan areas (Fig. 3). The NO_x emission rates of the major power plants within the Midwest
 3 simulated by SMOKE (Table S5) match well with the measurement from the Continuous Emission
 4 Monitoring System (CEMS) (de Foy et al., 2015; Duncan et al., 2013; Kim et al., 2009). The
 5 geographic distribution of grid-level annual NO_x emission density in our simulation also agrees

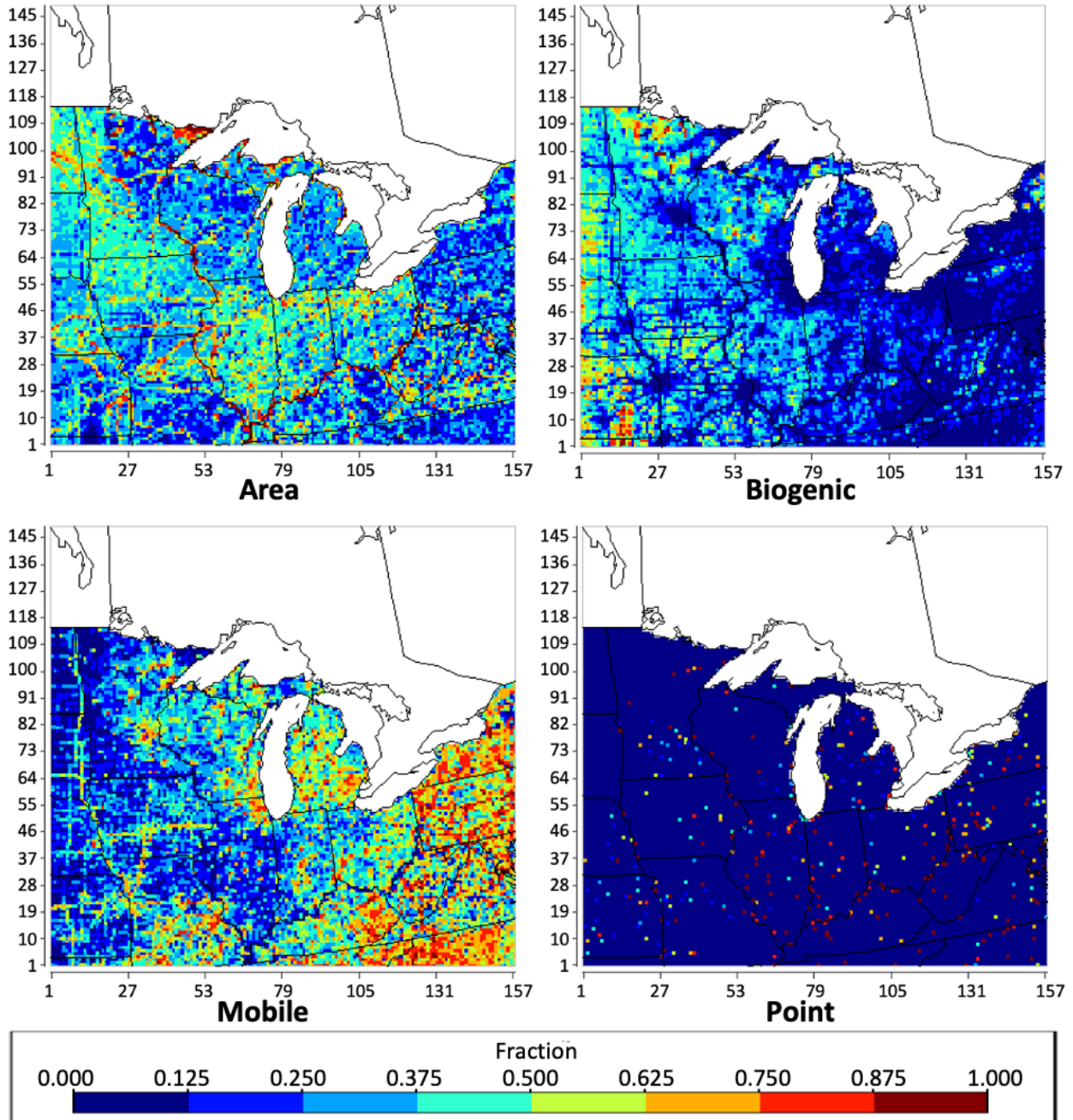


Figure 4: The geographical distribution of the fraction of NO_x emission from each SMOKE processing category (area, biogenic, mobile, point) over each grid throughout the Midwest between April and June based on NEI-2002.

1 with the county-level annual NO_x emission density discussed in the 2002 NEI booklet (Fig. S4;
2 USEPA, 2018b).

3 We next examine the spatial heterogeneity of the NO_x source fractions (Fig. 4) for the same
4 time period (April to June). The NO_x fraction (f) is defined as the amount of NO_x from a source
5 category (s) normalized to total NO_x ($f_s = \text{NO}_x(\text{source})/\text{NO}_x(\text{total})$). The fraction for anthropogenic
6 NO_x emission is defined as the amount of NO_x from a source category normalized to the sum of
7 NO_x emission from anthropogenic sources ($f_s = \text{NO}_x(\text{source})/(\text{NO}_x(\text{total}) - \text{NO}_x(\text{biogenic}))$). Since
8 the $\delta^{15}\text{NO}_x$ is determined by the NO_x emission fractions within each grid it is important to
9 understand where in the domain these fractions differ and why. The area sources, which mainly
10 consist of off-road vehicles, agriculture production, residential combustion, as well as the
11 industrial processes, which are individually too low in magnitude to report as point sources, are
12 fairly uniform in their distribution across the domain.

13 The SMOKE simulation shows that the f_s vary significantly across the domain. The average
14 area NO_x emission fraction (f_{area}) was 0.271 for total NO_x emission and 0.290 for anthropogenic
15 NO_x emission within the Midwest from April to June. The f_{area} 's show a clear spatial variation and
16 range from 0.125 to 0.5 over about 75% of the grids (Fig. S5). Geographically, the grids with
17 relatively higher f_{area} are in the rural area away from highways, where agricultural is the most
18 common land use classification. In the states of Wisconsin and Missouri, the f_{area} is slightly lower
19 due to the higher fraction of NO_x emission from biogenic sources (f_{biog}). In the states of
20 Pennsylvania and Michigan, the f_{area} is slightly lower due to the higher fraction of NO_x emission
21 from mobile sources (f_{mobile}). In addition, the grids with f_{area} greater than 0.75 are mainly located
22 along the Mississippi River and Ohio River, due to wastewater discharge. The f_{bio} shows a clear
23 spatial variation and is highest in the western portion of the domain (Fig. 4). The f_{bio} from April to
24 June is less than 0.5 in more than 90% of the grids within the geographic domain, with the average
25 of 0.065 (Fig. S5). Geographically, the grids with relatively high f_{bio} are located in the western
26 regions of the Midwest, away from cities and highway where the density of agricultural acreage
27 and natural vegetation is high. Furthermore, the lowest f_{bio} values occur in the megacities and along
28 the highways, which agrees well with the land-use related to the biogenic emission. The April to
29 June SMOKE simulation shows that f_{mobile} of 0.325 for total NO_x emission and 0.347 for
30 anthropogenic NO_x emission. The f_{mobile} shows a clear spatial variation, with relatively higher f_{mobile}
31 are located in major metropolitan regions and along the highways, where vehicles have the highest
32 density. The value of f_{mobile} within the geographic domain distributes evenly on the histogram (Fig.
33 S5). Based on the SMOKE simulation, the fraction of NO_x emission from point sources (f_{point}) is
34 0.339 for total NO_x emission and 0.363 for anthropogenic NO_x. The f_{point} 's are obviously highest
35 in grids where the power plants are located, mainly along the Ohio River valley and near other
36 water bodies close to metropolitan areas. The point sources occupy only 4% of the domain grids
37 and about 1/4 of the power plants are not at the same grids as highways, thus these grids have a
38 $f_{\text{point}} > 0.9$ NO_x.

39 40 3.2 Simulated spatial variability in $\delta^{15}\text{NO}_x$ 41

1
 2 Using these NO_x emission source
 3 fractions, the $\delta^{15}\text{NO}_x$ values were simulated
 4 and the spatial heterogeneity of $\delta^{15}\text{NO}_x$ for a
 5 single time period is discussed. The “emission
 6 only” simulation of $\delta^{15}\text{NO}_x$ values (at 06 UTC
 7 on July 26) ranged from -34.3‰ to 14.9‰
 8 (Fig. 5a). The majority of the grids have
 9 $\delta^{15}\text{NO}_x$ values lower than -16.3‰, which is
 10 due to biogenic NO_x emissions (-34.3‰) in
 11 sparsely populated areas where intensive
 12 agriculture dominates the land use (Fig. 5a).
 13 The $\delta^{15}\text{NO}_x$ values for grids containing big
 14 cities mainly ranged between -8.75‰ and -5‰
 15 due to the higher fraction of NO_x emission
 16 from on-road vehicles (-2.7‰), which also
 17 resolve major highways. The highest value of
 18 $\delta^{15}\text{N}$ occurs at the grids, where the coal-fired
 19 EGUs (+15‰) and hybrid-fired EGUs are the
 20 dominant NO_x source (Fig. 5a).

21 The effect of atmospheric mixing on the
 22 $\delta^{15}\text{NO}_x$ spatial distribution was then taken into
 23 account by coupling the $^{15}\text{NO}_x$ emissions to
 24 the meteorology simulation. There are
 25 significant differences between $\delta^{15}\text{NO}_x$ values
 26 in the “emission only” (Fig. 5a) and the
 27 “emission + transport” (Fig. 5b) simulations.
 28 While “emission only” $\delta^{15}\text{N}$ pattern shows
 29 biogenic NO_x emissions dominating the spatial
 30 domain, anthropogenic emissions become
 31 dominant over most of the grids in the
 32 “emission + transport” simulations, especially
 33 for the grids located around major cities and
 34 power plants. In general, as isotopically
 35 heavier urban NO_x disperses, the grid average
 36 increases from -20.2‰ under the “emission
 37 only” scenario to -11.5‰ under the “emission
 38 + transport” scenario. Similarly, the NO_x emitted
 39 along major highways is transported to the
 40 surrounding grids, so that the atmospheric NO_x
 41 at the grids around the major highways becomes
 42 isotopically heavier relative to the “emission only”
 43 scenario. We define $\Delta\delta^{15}\text{N}_{\text{transport}}$ as the $\delta^{15}\text{N}$
 44 difference between “emission only” and “emission +
 transport” scenarios. An example of the
 $\Delta\delta^{15}\text{N}_{\text{transport}}$ effect can be seen in grids
 encompassing a plume emanating from southern
 Illinois’ Baldwin Energy Complex (marked with a
 transparent white box on Fig. 5b) that uses
 subbituminous coal and bituminous coal as its
 major energy source. The $\Delta\delta^{15}\text{N}_{\text{transport}}$ in the
 regions

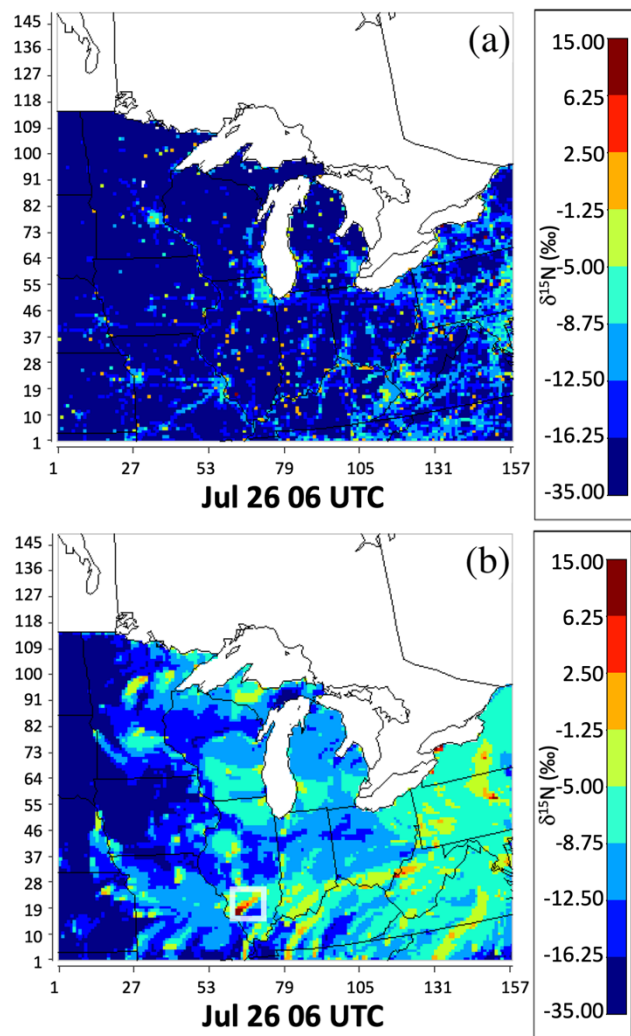


Figure 5: The $\delta^{15}\text{N}$ values of NO_x emission, (a: “emission only” scenario) and the $\delta^{15}\text{N}$ values of atmospheric NO_x based on NEI-2002 and 2016 meteorology (b: “emission + transport” scenario), at 06 UTC on July 26, are presented by color in each grid. The warmer the color, the higher $\delta^{15}\text{N}$ values of atmospheric NO_x . The feature of the transport inside the white box is shown in Fig. 6.

1 is altered as a function of distance away from
2 the EGU. In this time snapshot (06 UTC on
3 Jul 26), the northeastwards propagating
4 plume of NO_x emission from the EGU creates
5 higher $\delta^{15}\text{NO}_x$ over 135 km away (Fig. 6).

6 3.3 Seasonal variation in $\delta^{15}\text{NO}_x$

7 We next examine the temporal
8 heterogeneity of $\delta^{15}\text{NO}_x$ values over the
9 domain for “emission only” and interpret
10 them in terms of changes in NO_x emission
11 fractions as a function of time. The predicted
12 $\delta^{15}\text{NO}_x$ value for total emissions in the
13 Midwest during each season shows a
14 significant temporal variation (Fig. 7). The
15 $\delta^{15}\text{NO}_x$ ranged from -35‰ to 15‰, with the
16 annual average over the Midwest at -6.15‰.
17 The maps for different seasons show the
18 obvious changes in $\delta^{15}\text{N}$ values over western regions of the Midwest, going from -15 to -5‰ in
19 the spring to -35 to -15‰ in the summer. In order to qualitatively analyze the changes in $\delta^{15}\text{NO}_x$
20 among each season, the values over the grids (Fig. 7) were organized into the histograms (Fig. S6).
21 The grids with $\delta^{15}\text{NO}_x$ between -35‰ and -18‰ increase dramatically from less than 10% during
22 fall (Oct-Dec) and winter (Jan-Mar) to more than 20% during spring (Apr-Jun) and summer (Jul-
23 Sep). The grids with $\delta^{15}\text{NO}_x$ between -18‰ and -2‰ decrease from around 90% during fall and
24 winter to around 75% during spring and summer. The significant temporal variation in the $\delta^{15}\text{NO}_x$
25 during different seasons can be quantitatively explained by changing fractions of NO_x emission
26 from the biogenic source in any grid (Fig. S7) using Eq. (6). Unlike other NO_x emission sources,
27 the fraction of NO_x emission from biogenic sources changes significantly among each season
28 within the geographic domain, especially over the rural areas (Fig. S7).

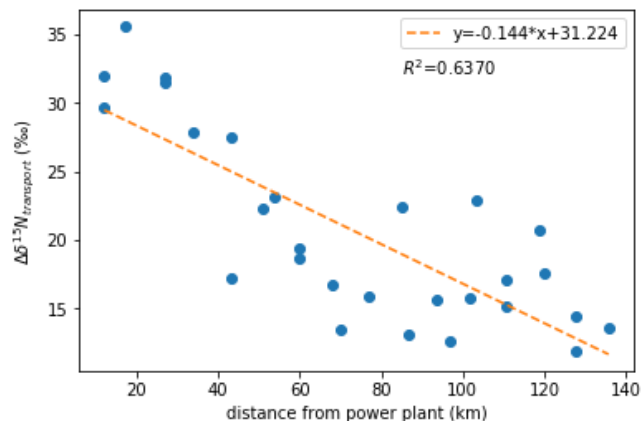


Figure 6: The $\Delta\delta^{15}\text{N}_{\text{transport}}$ along the plume (colored in dark red to orange inside the white box on Fig. 5b) over the distance from the power plant Baldwin Energy Complex (located at southwestern border of Illinois).

1

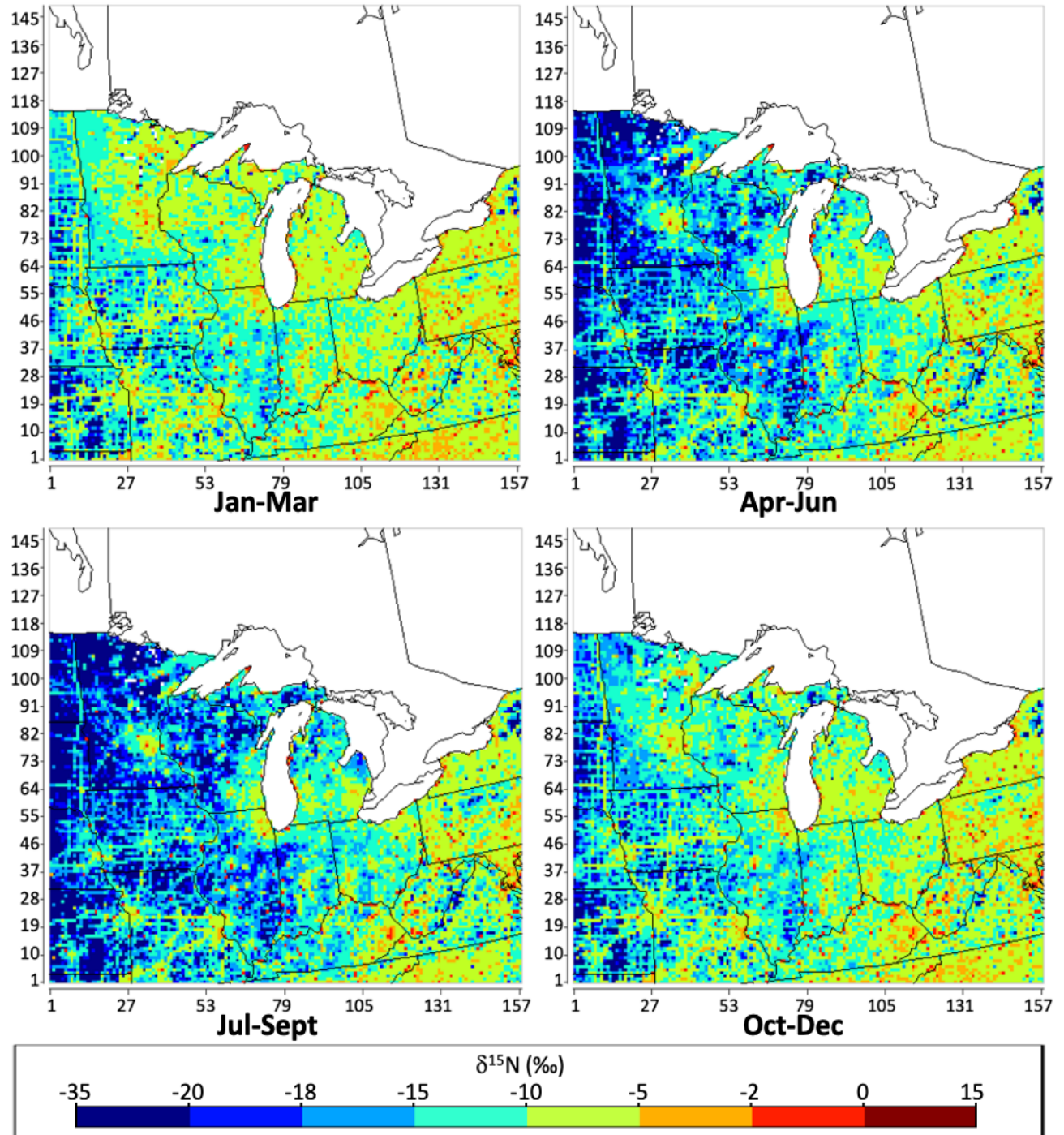


Figure 7: The geographical distribution of the $\delta^{15}\text{N}$ value of total NO_x emissions in each season (Winter: Jan-Mar; Spring: Apr-Jun; Summer: Jul-Sep; Fall: Oct-Dec) in per mil (‰) throughout the Midwest simulated by SMOKE, based on NEI-2002.

2

1 To qualitatively analyze the changes in the fraction of NO_x emission from biogenic sources
2 among each season, the distributions of the fractions among the same cut-offs as the maps on Fig.
3 S7 were shown in the histograms (Fig. S8). In general, the distribution of the fraction shifts to
4 higher values during spring (Apr-Jun) and summer (Jul-Sep), indicating the increase of biogenic
5 emissions. During this period, the surface sunlight hours, temperature, and precipitation are
6 relatively higher and as a result, the canopy coverage of the plants becomes higher, which leads to
7 the increase of the NO_x emission from biogenic sources (Pierce, 2001; Vukovich & Pierce, 2002;
8 Schwede et al., 2005; Pouliot & Pierce, 2009; USEPA, 2018a). Besides this, the fertilizer
9 application during this period is also increases soil NO_x emissions (Li & Wang, 2008; Felix &
10 Elliott, 2014). As a result, the distribution of δ¹⁵NO_x shifts to lower values during these periods
11 (Fig. 7). The percentage of the grids with the fraction of biogenic emission less than 0.125
12 decreases dramatically from more than 50% during fall (Oct-Dec) and winter (Jan-Mar) to less
13 than 35% during spring (Apr-Jun) and summer (Jul-Sep). As the NO_x emission from biogenic
14 source becomes dominant, the percentage of the grids with δ¹⁵NO_x between -35‰ and -18‰
15 increases, while the percentage of the grids with values between -18‰ and -2‰ decreases, which
16 sufficiently explains the trends shown on Fig. 7.

17 The temporal variation in atmospheric δ¹⁵NO_x is also controlled by the propagation of NO_x
18 emissions, which varies seasonally. The temporal heterogeneity of atmospheric δ¹⁵NO_x under the
19 “emission + transport” scenario is interpreted in terms of changes in the propagation of NO_x
20 emission as a function of time. The predicted seasonal average δ¹⁵NO_x in the Midwest shows
21 significant variations (Fig. 8). On an annual basis, the “emission + transport” average δ¹⁵NO_x value
22 was -6.10‰, which is similar to the “emission only” average range, but the range (-19.2‰ to
23 11.6‰) was narrower due to NO_x transport and mixing. The maps for different seasons show the
24 obvious changes in δ¹⁵N values over western regions of the Midwest, from -8.75 to -5‰ in fall
25 and winter to -16.25 to -12.5‰ in spring and summer. The spatial heterogeneity of the δ¹⁵NO_x
26 under the “emission + transport” scenario (Fig. 8) was compared to that under the “emission only”
27 scenario (Fig. 7). The difference was defined as Δδ¹⁵N_{transport} (Fig. S9) and had values ranged from
28 -21.9‰ to 31.2‰, with an average of 4.9‰. The grids with Δδ¹⁵N_{transport} between -5‰ and 0‰
29 are the urban areas and decrease slightly from about 11% during fall (Oct-Dec) and winter (Jan-
30 Mar) to 10% during spring (Apr-Jun) and summer (Jul-Sep). The grids with Δδ¹⁵N_{transport} between
31 0‰ and 5‰ are typically in the rural areas that are impacted by the urban NO_x emissions and
32 decrease dramatically from more than 50% during fall and winter to less than 40% during spring
33 and summer. The grids with Δδ¹⁵N_{transport} greater than 5‰, which are the rural areas obviously
34 impacted by the urban NO_x emission and increase dramatically from less than 40% during fall and
35 winter to more than 50% during spring and summer. Therefore, the impacts from transport and
36 mixing are more obvious during spring and summer (Fig. S10).

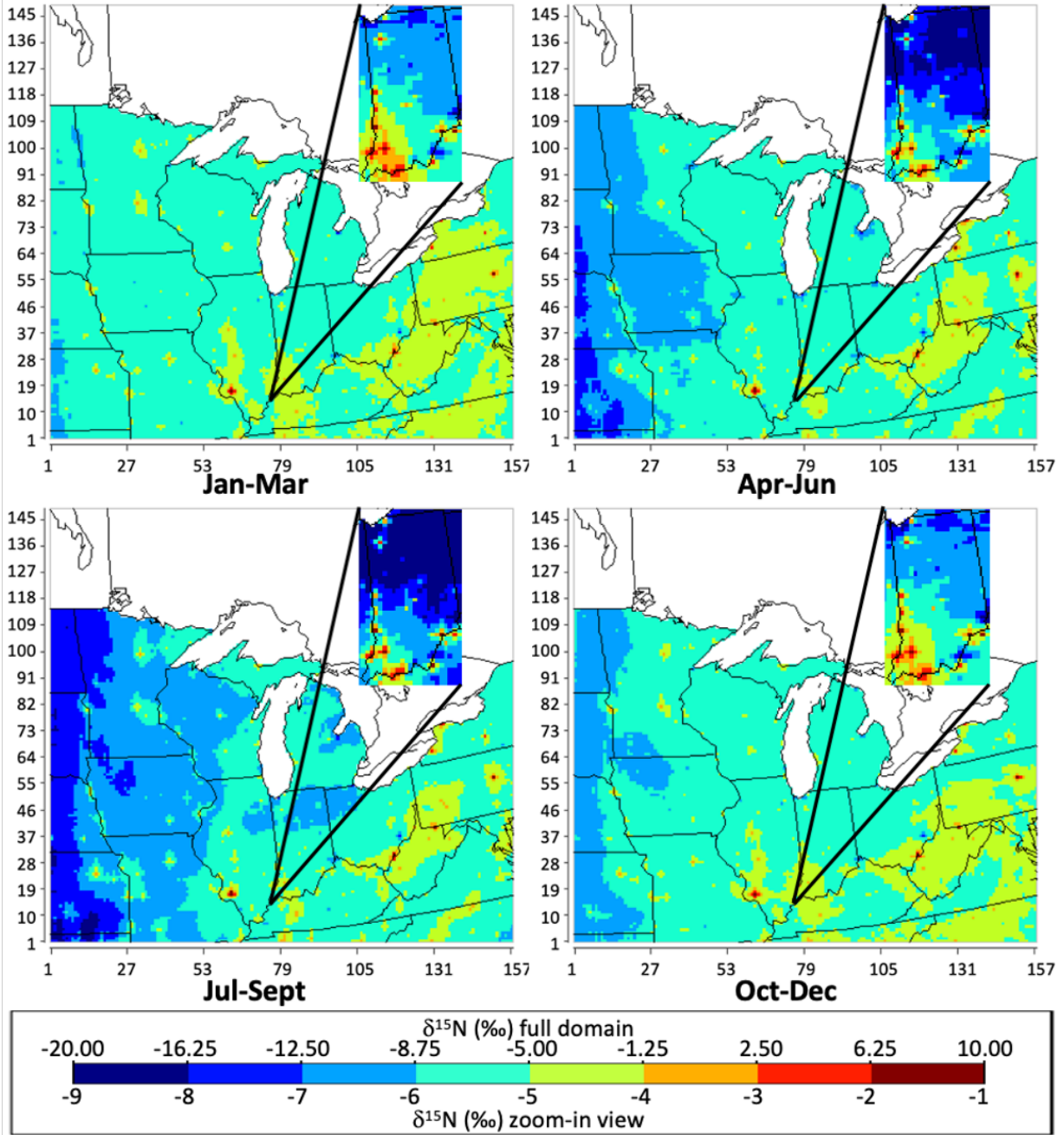


Figure 8: The geographical distribution of the $\delta^{15}\text{N}$ value of atmospheric NO_x in each season (Winter: Jan-Mar; Spring: Apr-Jun; Summer: Jul-Sep; Fall: Oct-Dec) in per mil (‰) throughout the Midwest (with zoom-in view focusing on Indiana) simulated by CMAQ, based on NEI-2002 and 2016 meteorology.

1

1 The PBL height is an effective indicator showing whether the pollutants are under synoptic
 2 conditions, which are favorable for the dispersion, mixing, and transport after being emitted into
 3 the atmosphere (Oke, 2002; Shu et al., 2017; Liao et al., 2018; Miao et al., 2019). Comparing the
 4 distributions $\Delta\delta^{15}\text{N}_{\text{transport}}$ values (Fig. S9) with the corresponding PBL height (Fig. S11) for each
 5 season, the effects of PBL height on the propagation of the air mass are clearly shown. NO_x emitted
 6 by power plants is much higher than the emission rates at the surrounding grids and is a hotspot
 7 that impacting the $\delta^{15}\text{N}$ values at the surrounding grids. As PBL increases, the emitted NO_x from
 8 power plant mixes more effectively with the surrounding grid, thus there are higher $\delta^{15}\text{NO}_x$ values
 9 along the power plant plume transect. The PBL height changes significantly among each season
 10 within the geographic domain, especially over Minnesota, Wisconsin, and Iowa (Fig. S11). The
 11 PBL height over these areas increases from less
 12 than 250 meters above the ground level to more
 13 than 625 meters above the ground level, during
 14 spring and summer, which creates a more
 15 favorable synoptic condition for the dispersion,
 16 mixing, and transport of the pollutants after being
 17 emitted into the atmosphere. As a result, the
 18 difference in $\delta^{15}\text{N}$ values shifts to higher values,
 19 showing the stronger effect of atmospheric
 20 processes during spring and summer. In order to
 21 qualitatively analyze how PBL height affects the
 22 $\delta^{15}\text{NO}_x$ along power plant plumes, the domain
 23 average PBL height for each month was plotted
 24 against $\delta^{15}\text{NO}_x$ (Fig. 9a). The $\delta^{15}\text{N}$ values along
 25 the power plants plumes and PBL heights over
 26 the domain have the same seasonal trend.
 27 Interestingly, the “turning point” of the $\delta^{15}\text{N}$
 28 values is about one month later than the “turning
 29 point” of the PBL heights. The scatter plot (Fig.
 30 9b) shows a strong positive correlation ($R^2=0.85$)
 31 between the domain average PBL height and
 32 average $\delta^{15}\text{N}$ value along the power plants
 33 plumes. The positive correlation between PBL
 34 height and propagation of air mass, indicated by
 35 the evolution of atmospheric $\delta^{15}\text{NO}_x$ in this
 36 study, agrees well with the corresponding
 37 measurement in megacities in China from the
 38 previous studies (Shu et al., 2017; Liu et al.,
 39 2018; Liao et al., 2018).

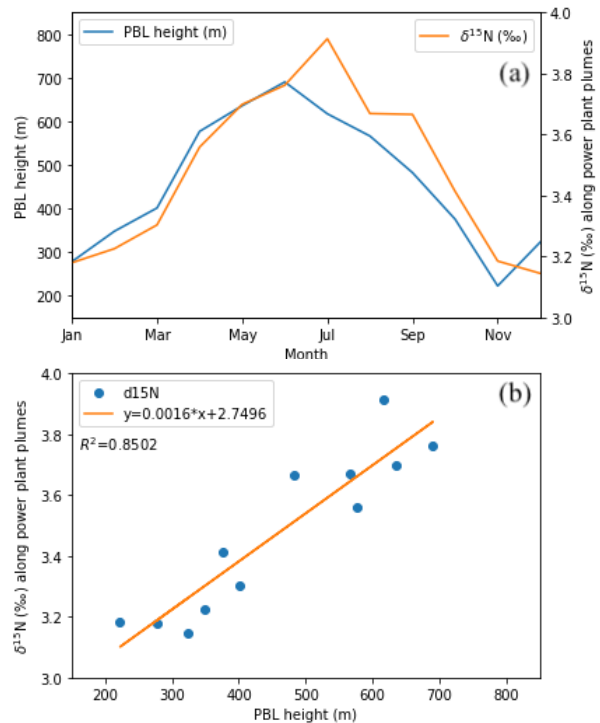


Figure 9: The time series plot (a) and the scatter plot (b) of the domain average PBL height (m) and the average $\delta^{15}\text{N}$ (%) value of atmospheric NO_x along the plumes of power plants during each month throughout the Midwest simulated by CMAQ, based on NEI-2002 and 2016 meteorology.

1
 2 3.4 The simulations based on different meteorology input datasets
 3 The spatial heterogeneity of the $\delta^{15}\text{NO}_x$ using 2016 meteorology input dataset was compared
 4 to that using 2002 meteorology (Fig. S13). Overall, the simulated $\delta^{15}\text{NO}_x$ using 2002 meteorology
 5 has the similar geographic distribution and seasonal trend as the 2016 simulation. The difference
 6 was defined as $\Delta\delta^{15}\text{N}_{2002-2016}$ (Fig. 10) and had values ranged between -1.25‰ and $+1.25\text{‰}$ over
 7 most of the grids. However, in the western part of the domain, where the biogenic NO_x emission

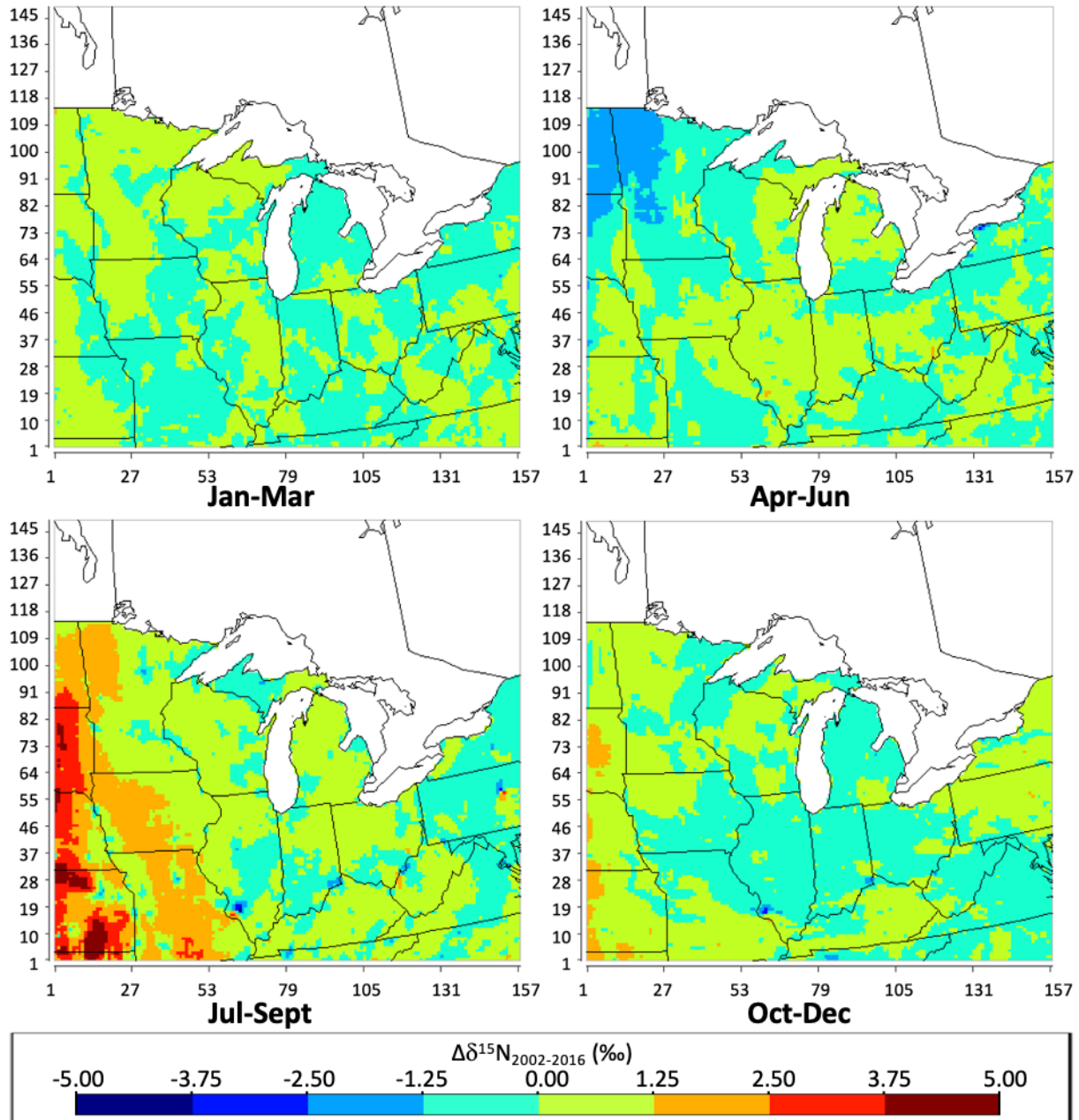


Figure 10: The difference between the $\delta^{15}\text{N}$ (‰) value of atmospheric NO_x based on 2016 meteorology and 2002 meteorology ($\Delta\delta^{15}\text{N}_{2002-2016}$) during each season (Winter: Jan-Mar; Spring: Apr-Jun; Summer: Jul-Sep; Fall: Oct-Dec), throughout the Midwest simulated by CMAQ.

1 is dominant, the more positive $\Delta\delta^{15}\text{N}_{2002-2016}$ values (up to 5‰) during summer and fall occur. On
 2 the other hand, the more negative $\Delta\delta^{15}\text{N}_{2002-2016}$ values (up to -5‰) occur along the power plant
 3 plume during the same period. The spatial heterogeneity of $\Delta\delta^{15}\text{N}_{2002-2016}$ indicates how climate
 4 change alters the $\delta^{15}\text{NO}_x$. If we have enough input datasets to generate and compare the
 5 seasonal/monthly $\delta^{15}\text{NO}_x$ over the past 20+ years, the impacts of anomalies in each meteorology
 6 variables could be explored. For the current dataset, the similar comparison between the $\delta^{15}\text{NO}_x$
 7 and the corresponding PBL height was conducted for the simulation based on 2002 meteorology
 8 (Fig. S14) to show how PBL height changes the evolution of $\delta^{15}\text{NO}_x$. Under the 2002 meteorology,
 9 lower PBL height during the winter caused surface $\delta^{15}\text{NO}_x$ values along the power plants' plumes
 10 to be lower relative to 2016 meteorology. On the other hand, due to the higher PBL height during
 11 the 2002 spring and summer the $\delta^{15}\text{N}$ values decreased through July before ending with the
 12 relatively higher $\delta^{15}\text{N}$ values in December. The scatter plot for the simulation based on 2002
 13 meteorology (Fig. S14b) also shows a strong positive correlation between the domain average PBL
 14 height and average $\delta^{15}\text{N}$ value along the power plants plumes, with $R^2=0.78$. The videos of
 15 atmospheric $\delta^{15}\text{NO}_x$ on an hourly basis throughout the years 2002 and 2016 are available on
 16 Zenodo.org (10.5281/zenodo.4311986).

17

18 3.5 The simulation over the extracted domain

19 Analysis of the whether there was difference between the extracted-domain simulation (Fig.
 20 2) and full-domain simulation was conducted by defining $\Delta\delta^{15}\text{N}_{\text{extracted-full}}$ and assessing the bias
 21 due to the motion of the air mass across the domain boundary (Fig. S17). The $\Delta\delta^{15}\text{N}_{\text{extracted-full}}$
 22 values ranged between -0.25‰ and +0.25‰ over most of the grids, showing the difference
 23 between extracted-domain simulation and full-domain simulation of $\delta^{15}\text{N}$ values are usually trivial.
 24 However, near the southern border of the extracted domain $\Delta\delta^{15}\text{N}_{\text{extracted-full}}$ values close to +0.75‰
 25 (fall and winter) and close to +1.00‰ (spring and summer) suggesting extracted domain may be
 26 required for accurate $\delta^{15}\text{NO}_x$ simulations

27

28 3.6 The role of enhanced NO_x loss

29 The “emission + transport + enhanced NO_x
 30 loss” simulations significantly alter the $\delta^{15}\text{NO}_x$
 31 relative to the “normal deposition” scenarios.
 32 Again, the enhanced NO_x loss cases are removing
 33 NO_x at rates similar to those by removal via its
 34 conversion into HNO_3 . Thus, the NO_x deposited is
 35 $\sim \delta^{15}\text{NO}_3^-$ (assuming no photochemical isotope
 36 effects) and the $\delta^{15}\text{NO}_x$ is that in the residual NO_x .
 37 The impact of enhanced NO_x loss on the residual
 38 NO_x was assessed using $\Delta\delta^{15}\text{N}_{\text{hi-no}}$, the difference
 39 between the $\delta^{15}\text{NO}_x$ values under the “enhanced
 40 NO_x loss” and “no deposition” scenarios. The
 41 $\Delta\delta^{15}\text{N}_{\text{hi-no}}$ range was $\pm 4\text{‰}$ and was especially
 42 obvious downwind of the locations with large
 43 emission rates, such as power plants or megacities
 44 (Fig. 11). This can be explained in a similar
 45 fashion to the “no deposition” scenarios (Fig. S18a), where the dispersion of the isotopically

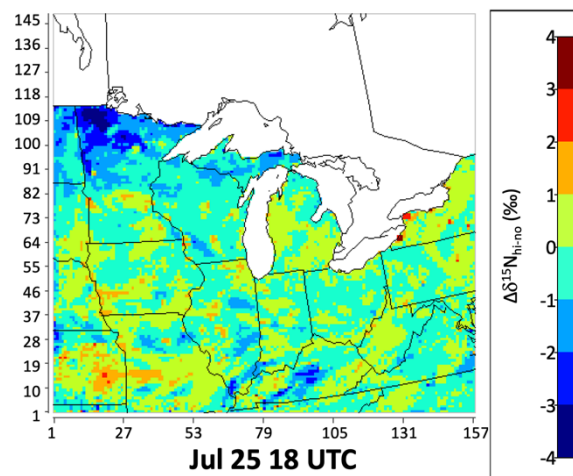


Figure 11. The $\Delta\delta^{15}\text{N}_{\text{hi-no}}$ values at 18 UTC on July 25.

1 heavier NO_x emission from big cities, major highways, and power plants elevated the $\delta^{15}\text{NO}_x$
2 values in rural areas and the dispersion of the isotopically lighter biogenic NO_x emission lowered
3 the $\delta^{15}\text{NO}_x$ values in the surrounding grids located in the suburb of major cities (Fig. S18b). When
4 “enhanced NO_x loss” is used the transport, mixing, and dispersion of local NO_x emissions are
5 restricted to smaller geographical extent (Fig. S18b) leading to different $\delta^{15}\text{NO}_x$ values relative to
6 no deposition. The temporal heterogeneity of $\Delta\delta^{15}\text{N}_{\text{hi-no}}$ over the domain was examined and the
7 impact of enhancing deposition rates of NO_x on the $\delta^{15}\text{N}$ of atmospheric NO_x on a seasonal basis
8 was explored (Fig. 12). The seasonal $\Delta\delta^{15}\text{N}_{\text{hi-no}}$ values range from -3.67‰ to 5.34‰, with an
9 average of 0.51‰. The overall pattern of the $\Delta\delta^{15}\text{N}_{\text{hi-no}}$ values shows that due to deposition, the
10 atmospheric NO_x became isotopically lighter over the majority of the grids since EGU and vehicle
11 NO_x is not being transported as far. Conversely, in grids that contain or surround power plants and
12 big cities the $\delta^{15}\text{NO}_x$ increases because it is not as effectively mixing with low $\delta^{15}\text{NO}_x$ from nearby
13 grids. The enhanced NO_x loss simulation was used as a proxy to present the isotope effects
14 associated with the “pseudo photochemical transformation” of NO_x into NO_y . The complete
15 isotope effect of tropospheric photochemistry will be addressed in future work, which incorporates
16 ^{15}N into the chemical mechanism of CMAQ for the simulation.

17 The $\delta^{15}\text{NO}_x$ value of dry deposition (a proxy for $\delta^{15}\text{NO}_3^-$) simulated by CMAQ show similar
18 monthly variations and seasonal trends as SMOKE (Fig. S22). The ranges of $\delta^{15}\text{NO}_x$ values within
19 each month were narrower, compared to the simulation from SMOKE, with a minimum during
20 February (-8.7~ -4.4‰) and a maximum during August (-11.8~-4.2‰). The seasonal trend shows
21 low $\delta^{15}\text{NO}_x$ values in deposition during summer, with the median around -7.4‰, and slightly
22 higher values during winter (median around -6.0‰). Therefore, the CMAQ simulation inherits the
23 monthly variations and seasonal trends from SMOKE, while the atmospheric NO_x becomes
24 isotopically heavier, after taking atmospheric mixing and transport into account. As mentioned
25 above, most of the NADP sites are located away from big cities and power plants. Thus, the
26 atmospheric mixing and transport led to the isotopically heavier atmospheric NO_x .

27

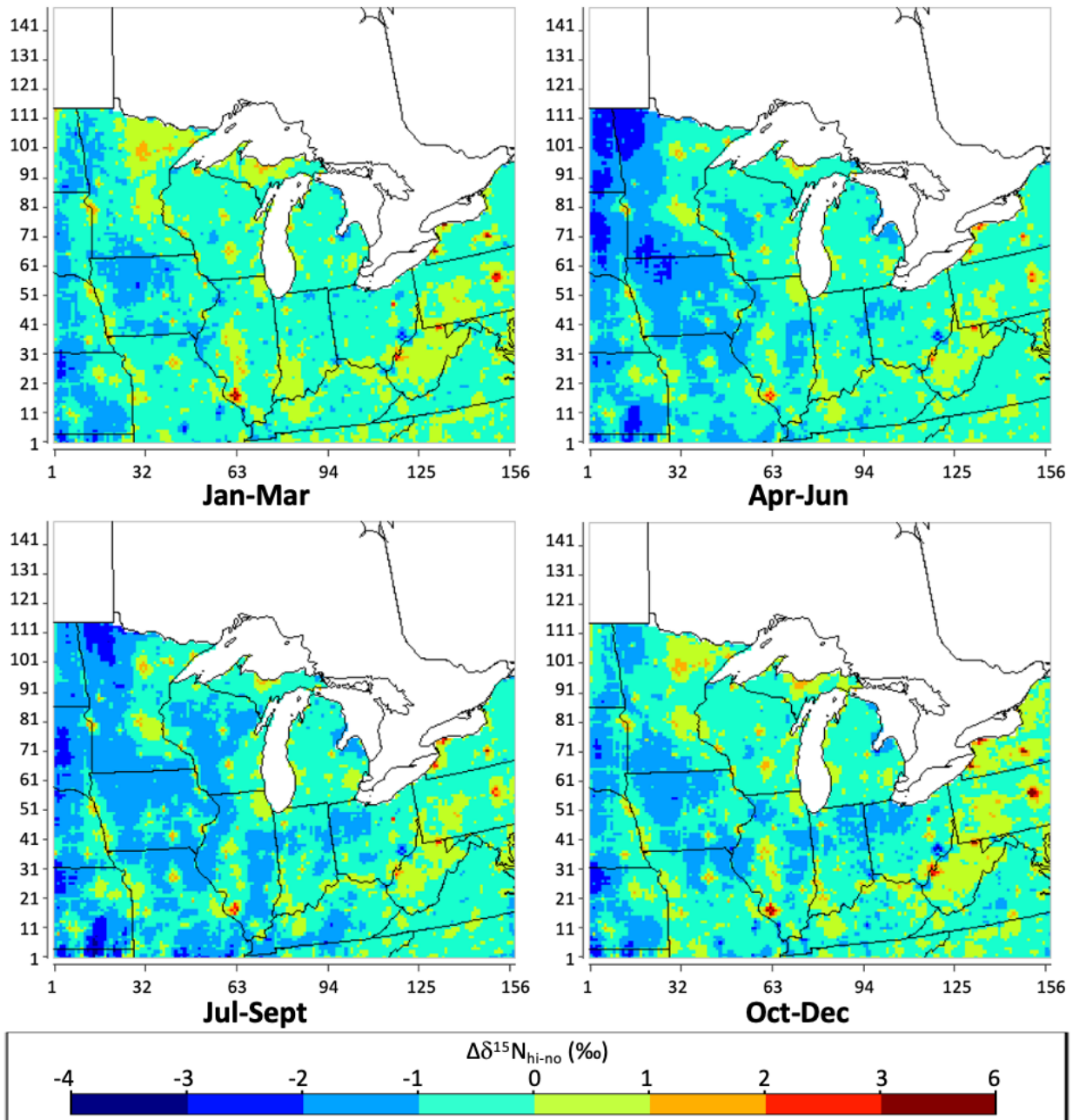


Figure 12: The difference between the $\delta^{15}\text{N}$ (‰) value of atmospheric NO_x under the “enhanced NO_x loss” scenario and “no deposition” scenario ($\Delta\delta^{15}\text{N}_{\text{hi-no}}$) during each season (Winter: Jan-Mar; Spring: Apr-Jun; Summer: Jul-Sept; Fall: Oct-Dec), throughout the Midwest simulated by CMAQ, based on NEI-2002 and 2016 meteorology.

1
2
3
4

3.7 Model-observation comparison of $\delta^{15}\text{NO}_x$

1 In order to evaluate the
 2 SMOKE/CMAQ simulations of
 3 atmospheric $\delta^{15}\text{NO}_x$, they were
 4 compared to two recent studies of
 5 $\delta^{15}\text{NO}_x$. The first comparison was
 6 relative to rainwater measurements in
 7 West Lafayette, IN from July 9 to
 8 August 5, 2016 (Walters, Fang, &
 9 Michalski, 2018). The measured $\delta^{15}\text{NO}_x$
 10 values ranged from -33.8‰ to 0.2‰,
 11 with the median of -11.2 ± 8.02 ‰. Under
 12 the “emission + transport + enhanced
 13 NO_x loss” scenario using 2016
 14 meteorology, the simulated $\delta^{15}\text{NO}_x$
 15 mean (-7.9 ± 2.19 ‰) was 3.3‰ less
 16 negative than the observations and the
 17 range (-15.9 ‰ to -3.7 ‰) was about half
 18 that in the observations (Fig. 13, top,
 19 Table S7). The predicted $\delta^{15}\text{NO}_x$ was
 20 similar regardless of whether 2016 or
 21 2002 meteorology was used but were
 22 closer to the measured values,
 23 comparing to the “emission only”
 24 simulations (Fig. 13, top). It is not
 25 surprising that the measurements are
 26 more negative than the observations
 27 because the model does not account for
 28 isotope fractionation during the
 29 conversion NO_x into NO_y . Our previous
 30 work has shown the photochemical
 31 isotope effect enriches NO_y and depletes
 32 NO_x (Fang et al., 2021; Walters and
 33 Michalski, 2015) and thus the lower
 34 measured $\delta^{15}\text{NO}_x$ relative to model is
 35 consistent with this isotopic depletion.

36 Our model simulations were also compared to on-road vehicle plume measurement along Midwest highways from August 8 to 18, 2015 (Miller et al., 2017). The boxplot also shows more accurate estimation of $\delta^{15}\text{N}$ after considering the atmospheric mixing with the emission from surrounding grids (Fig. 13, bottom). Using the “emission only” scenario, the simulated $\delta^{15}\text{NO}_x$ mean was about 3‰ more negative than the observations. The predicted $\delta^{15}\text{NO}_x$ under the “emission + transport + enhanced NO_x loss” scenario for these samples along Midwest highways was closer to the measured values, compared to the “emission only” simulations, using no matter 2016 or 2002 meteorology. The modeled values are quite close to the observations suggesting the photochemical isotope effect is small for these samples. This is not surprising given they were collected on major highways where NO_x concentrations are high and the timescale between collection and emission

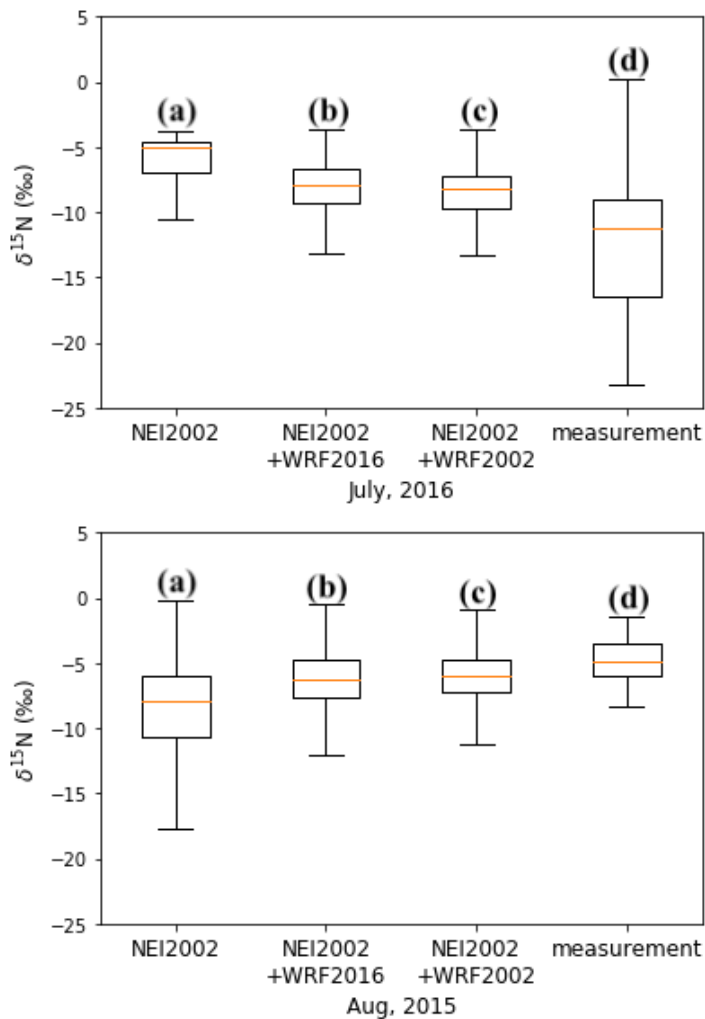


Figure 13: The $\delta^{15}\text{NO}_x$ distributions at Lafayette, IN (top) and along Midwest highways (bottom), simulated by SMOKE (a), CMAQ based on 2016 (b) and 2002 meteorology (c), compare with the measured $\delta^{15}\text{NO}_x$ (d) (box: lower quartile, median, upper quartile; whisker: lower extreme, upper extreme)

1 is small and thus only a small fraction of emitted NO_x would have been converted to NO_y
2 minimizing the photochemical isotope effect.

3 The 30 fold enhanced NO_x loss (see methods) was used to simulate the $\delta^{15}\text{N}$ value of NO_3^-
4 deposition ($\delta^{15}\text{NO}_3^-$) that was then compared to observations (Fig. 14). As previously noted, rather
5 than explicitly converting NO_x into NO_y via the chemical mechanism in CMAQ, which would
6 require writing an isotope-enabled chemical scheme with appropriate rate constants, we amplified
7 NO_x deposition as a surrogate. This amplification reduced the NO_x lifetime to about 1 day, thus
8 by calculating the $\delta^{15}\text{NO}_x$ in the deposition fraction, as opposed to residual NO_x in the atmosphere,
9 we are approximating the $\delta^{15}\text{NO}_3^-$ in deposition. The simulated $\delta^{15}\text{NO}_3^-$ was compared to NO_3^-
10 collected at NADP sites within Indiana, Illinois, and Ohio in the year 2002 (Table S4). The NEI-
11 2002 and WRF2002 were used for the SMOKE emission model and CMAQ simulations,
12 respectively. The value in deposition was calculated by $\delta^{15}\text{NO}_3^- = \sum f_{\text{NO}_x\text{hr}} \delta^{15}\text{NO}_{x\text{hr}}$, where $f_{\text{NO}_x\text{hr}}$
13 is the hourly mole fraction of NO_x isotopologue deposited ($f_{\text{NO}_x\text{hr}} = \text{NO}_{x\text{hr}}/\text{NO}_{x\text{T}}$) and $\delta^{15}\text{NO}_{x\text{hr}}$ is
14 the $\delta^{15}\text{N}$ value of NO_x in deposition. The total NO_x deposited ($\text{NO}_{x\text{T}}$) used to calculate $f_{\text{NO}_x\text{hr}}$ was
15 the amount deposited 5 days prior to the sampling date since the NADP deposition collection
16 integrate the week.

17 The $\delta^{15}\text{N}$ values of NO_x
18 deposition simulated by CMAQ
19 under the “emission + transport +
20 enhanced NO_x loss” scenario at
21 each site were compared with the
22 measurements of $\delta^{15}\text{N}$ values of
23 NO_3^- from prior studies (Mase,
24 2010; Riha, 2013). While the
25 scatter plot shows a moderate
26 positive correlation between
27 observed and simulated $\delta^{15}\text{NO}_3^-$,
28 the simulated value is consistently
29 lighter than the sample $\delta^{15}\text{NO}_3^-$
30 (Fig. 14, top). The magnitude of
31 this negative bias varies among the
32 NADP sites (Fig. S23) and is
33 attributed to isotope fractionation
34 during the conversion NO_x into
35 NO_y , which enriches NO_3^- (Fang et
36 al., 2021; Walters and Michalski,
37 2015). Globally this enrichment
38 has been estimated at $3.9 \pm 1.8\text{‰}$
39 (Song et al, 2021). But this
40 enrichment is a function of NO_x ,
41 VOC, and oxidant loading, as well
42 as temperature, and photolysis rate
43 (Fang et al., 2021) and is not
44 expected to be the same at each
45 NADP site. After adjusting the
46 simulated $\delta^{15}\text{N}$ by raising the values by the average of the difference between sample $\delta^{15}\text{N}$ and

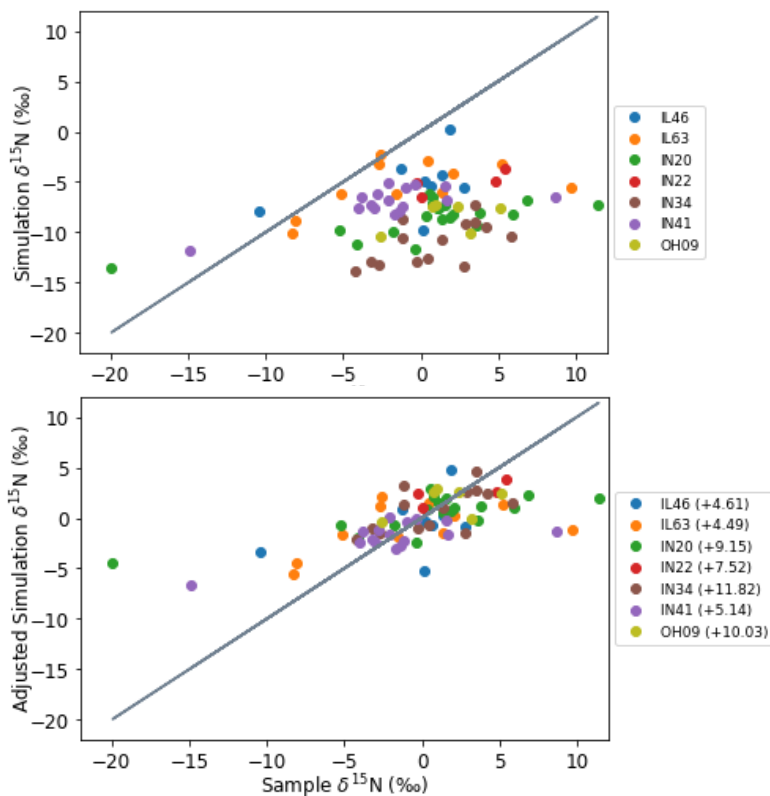


Figure 14: The emission + transport + enhanced NO_x loss CMAQ predicted $\delta^{15}\text{N}$ value of NO_x deposition using NEI-2002 and 2002 meteorology compared to the measured $\delta^{15}\text{N}$ of rain NO_3^- at NADP sites within IN, IL, and OH. The photochemical isotope enrichment factor (‰) correction used for each site is noted in the legend.

1 simulated $\delta^{15}\text{N}$ for each site, the scatter plots of sample $\delta^{15}\text{N}$ vs. simulated $\delta^{15}\text{N}$ well fit into the
2 one-to-one line (Fig. 14, bottom). The complete ^{15}N incorporated chemical mechanisms will be
3 explored in future study.

4 5 4. Conclusion

6 The evolution of $\delta^{15}\text{N}$ values along the “journey” of atmospheric NO_x were traced, using our
7 ^{15}N incorporated SMOKE and CMAQ. The $\delta^{15}\text{NO}_x$ under the “emission only” scenario was
8 simulated by SMOKE, using the NO_x emissions from NEI emission sectors and the corresponding
9 $\delta^{15}\text{N}$ values from previous research. The SMOKE simulation indicates that the NO_x emission from
10 biogenic sources is the key driver for the variation of $\delta^{15}\text{N}$, especially among the Midwestern
11 NADP sites. The uncertainties in the $\delta^{15}\text{NO}_x$ emission are less than 5‰ over the majority of the
12 grids within the Midwest, which were well below the difference among the assigned $\delta^{15}\text{NO}_x$ values
13 for different NO_x emission sources (Fig. S24). The $\delta^{15}\text{NO}_x$ under the “emission + transport”
14 scenario was simulated by CMAQ, using the ^{15}N incorporated emission input dataset generated
15 from SMOKE, as well as the meteorology input dataset generated from WRF and MCIP. The
16 CMAQ simulation indicates that the PBL height is the key driver for the mixture of anthropogenic
17 and natural NO_x emission, which deepens the gap between $\delta^{15}\text{N}$ of atmospheric NO_x and NO_x
18 emission. The $\delta^{15}\text{NO}_x$ under the “emission + transport + enhanced NO_x loss” scenario was
19 simulated by enhancing NO_x deposition in CMAQ simulation, to show how “lifetime chemistry”
20 alters $\delta^{15}\text{NO}_x$ values before it can be transported along significant distances, assuming no isotope
21 fractionation during chemical conversion or deposition.

22 The simulations under “emission only” scenario and “emission + transport + enhanced NO_x
23 loss” scenario were compared to the measurements in West Lafayette, Indiana. The simulated $\delta^{15}\text{N}$
24 agreed well with the seasonal trend and monthly variation. The simulated $\delta^{15}\text{NO}_x$ under the
25 “emission only” scenario was less negative than the corresponding measurements in West
26 Lafayette, IN, taken from July to August 2016. Thus, if we only consider the effects from NO_x
27 emission sources, the emission from soil, livestock waste, off-road vehicles, and natural gas power
28 plant in West Lafayette, IN are possible to be underestimated, and the emission from the on-road
29 vehicle and coal-fired power plant in West Lafayette, IN are possibly overestimated. The simulated
30 $\delta^{15}\text{NO}_x$ under the “emission + transport + enhanced NO_x loss” scenario was about 3‰ closer to
31 the corresponding measurements in West Lafayette, IN, comparing to the “emission only”
32 simulations. The simulations under “emission + transport + enhanced NO_x loss” scenario was also
33 compared to the measurements of $\delta^{15}\text{NO}_3^-$ from NADP sites within Indiana, Illinois, Ohio, and
34 Kentucky. The sample-by-sample comparison shows a moderate positive correlation between
35 observed and simulated $\delta^{15}\text{NO}_3^-$, with negative bias varies among the NADP sites. This bias is
36 attributed to isotope fractionation during the conversion NO_x into NO_y , affected by different NO_x ,
37 VOC, and oxidant loading, as well as temperature, and photolysis rate at each NADP site.
38 Therefore, the future work is to explore how tropospheric photochemistry alters $\delta^{15}\text{NO}_x$ by
39 incorporating ^{15}N into the chemical mechanism of CMAQ and comparing the simulation with the
40 corresponding measurements. With the validation of our nitrogen isotopes incorporated CMAQ,
41 the NO_x emission inventories could be effectively evaluated and improved.

1 **Data availability:** The source code for SMOKE version 4.6 is available at
2 https://github.com/CEMPD/SMOKE/releases/tag/SMOKEv46_Sep2018. The source code for
3 CMAQ version 5.2.1 is available at <https://github.com/USEPA/CMAQ/tree/5.2.1>. The in-detail
4 simulation results for $\delta^{15}\text{N}$ of NO_x emission based on 2002 and 2016 versions of National Emission
5 Inventory and the associated python codes are achieved on Zenodo.org (10.5281/zenodo.4048992).
6 The input datasets for WRF simulation are available at <https://www.ncei.noaa.gov/data/>. The in-
7 detail simulation results for $\delta^{15}\text{N}$ of atmospheric NO_x under all scenarios discussed in this paper
8 and the CMAQ-based c-shell script for generating BCON for extracted domain simulation are
9 achieved on Zenodo.org (10.5281/zenodo.4311986).

10
11 **Author contributions:** Huan Fang and Greg Michalski were the investigator for the project and
12 organized the tasks. Huan Fang develop the model codes, performed the simulation to incorporate
13 ^{15}N into SMOKE outputs and generated $\delta^{15}\text{N}$ values and reconstruct CMAQ by incorporating ^{15}N ,
14 and performed the simulation to generate $\delta^{15}\text{N}$ values. Greg Michalski helped Huan Fang in
15 interpreting the results. Huan Fang prepared the manuscript with contributions from all co-authors.

16
17 **Acknowledgments:** We would like to thank the Purdue Research Foundation, the Purdue Climate
18 Change Research Center, and the National Science Foundation (AGS award 1903646) for
19 providing funding for the project. We would like to thank Scott Spak from School of Urban &
20 Regional Planning, University of Iowa for simulating SMOKE using NEI-2002. We would like to
21 thank Tomas Ratkus from Department of Earth, Atmospheric, and Planetary Sciences, Steven Plite,
22 and Frank Bakhit from Rosen Center for Advanced Computing, Purdue University for setting up
23 CMAQ on Purdue research computing for this project.

1 **References:**

2 Almaraz, M., Bai, E., Wang, C., Trousdell, J., Conley, S., Faloona, I. and Houlton, B. Z.:
3 Agriculture is a major source of NO_x pollution in California, *Sci. Adv.*,
4 doi:10.1126/sciadv.aao3477, 2018.

5
6 Ammann, M., Siegwolf, R., Pichlmayer, F., Suter, M., Saurer, M. and Brunold, C.: Estimating
7 the uptake of traffic-derived NO₂ from 15N abundance in Norway spruce needles, *Oecologia*,
8 doi:10.1007/s004420050710, 1999.

9
10 Beirle, S., Spichtinger, N., Stohl, A., Cummins, K. L., Turner, T., Boccippio, D., Cooper, O. R.,
11 Wenig, M., Grzegorski, M., Platt, U. and Wagner, T.: Estimating the NO_x produced by lightning
12 from GOME and NLDN data: A case study in the Gulf of Mexico, *Atmos. Chem. Phys.*,
13 doi:10.5194/acp-6-1075-2006, 2006.

14
15 Boersma, K. F., Eskes, H. J., Meijer, E. W. and Kelder, H. M.: Estimates of lightning NO_x;
16 production from GOME satellite observations, *Atmos. Chem. Phys.*, doi:10.5194/acp-5-2311-
17 2005, 2005.

18
19 Bradshaw, J., Davis, D., Grodzinsky, G., Smyth, S., Newell, R., Sandholm, S. and Liu, S.:
20 Observed distributions of nitrogen oxides in the remote free troposphere from the NASA Global
21 Tropospheric Experiment programs, *Rev. Geophys.*, doi:10.1029/1999RG900015, 2000.

22
23 Byun, D., Pleim, J., Tang, R. and Bourgeois, A.: Meteorology-Chemistry Interface Processor
24 (MCIP) for Models-3 Community Multiscale Air Quality (CMAQ) Modeling System, System,
25 1999.

26
27 Chameides, W. L., Davis, D. D., Bradshaw, J., Rodgers, M., Sandholm, S. and Bai, D. B.: An
28 estimate of the NO_x production rate in electrified clouds based on NO observations from the
29 GTE/CITE 1 fall 1983 field operation, *J. Geophys. Res.*, doi:10.1029/jd092id02p02153, 1987.

30
31 Chang, Y., Zhang, Y., Tian, C., Zhang, S., Ma, X., Cao, F., Liu, X., Zhang, W., Kuhn, T. and
32 Lehmann, M. F.: Nitrogen isotope fractionation during gas-to-particle conversion of NO_x to
33 NO₃⁻ in the atmosphere - Implications for isotope-based NO_x source apportionment, *Atmos.*
34 *Chem. Phys.*, doi:10.5194/acp-18-11647-2018, 2018.

35
36 Christian, H. J., Blakeslee, R. J., Boccippio, D. J., Boeck, W. L., Buechler, D. E., Driscoll, K. T.,
37 Goodman, S. J., Hall, J. M., Koshak, W. J., Mach, D. M. and Stewart, M. F.: Global frequency
38 and distribution of lightning as observed from space by the Optical Transient Detector, *J.*
39 *Geophys. Res. Atmos.*, doi:10.1029/2002jd002347, 2003.

40
41 Cicero-Fernández, P., Long, J. R. and Winer, A. M.: Effects of Grades and Other Loads on On-
42 Road Emissions of Hydrocarbons and Carbon Monoxide, *J. Air Waste Manag. Assoc.*,
43 doi:10.1080/10473289.1997.10464455, 1997.

44
45 Dameris, M., Grewe, V., Ponater, M., Deckert, R., Eyring, V., Mager, F., Matthes, S., Schnadt,
46 C., Stenke, A., Steil, B., Brühl, C. and Giorgetta, M. A.: Long-term changes and variability in a

1 transient simulation with a chemistry-climate model employing realistic forcing, *Atmos. Chem.*
2 *Phys.*, doi:10.5194/acp-5-2121-2005, 2005.
3
4 Davidson, E. A.: Pulses of nitric oxide and nitrous oxide flux following wetting of dry soil: an
5 assessment of probable sources and importance relative to annual fluxes, *Trace gas Exch. a Glob.*
6 *Perspect.*, 1992.
7
8 Davidson, E. A. and Kingerlee, W.: A global inventory of nitric oxide emissions from soils,
9 *Nutr. Cycl. Agroecosystems*, doi:10.1023/a:1009738715891, 1997.
10
11 de Foy, B., Lu, Z., Streets, D. G., Lamsal, L. N. and Duncan, B. N.: Estimates of power plant
12 NO_x emissions and lifetimes from OMI NO₂ satellite retrievals, *Atmos. Environ.*,
13 doi:10.1016/j.atmosenv.2015.05.056, 2015.
14
15 De Laeter, J. R., Böhlke, J. K., De Bièvre, P., Hidaka, H., Peiser, H. S., Rosman, K. J. R. and
16 Taylor, P. D. P.: Atomic weights of the elements: Review 2000 (IUPAC Technical Report), *Pure*
17 *Appl. Chem.*, doi:10.1351/pac200375060683, 2003.
18
19 DeCaria, A. J., Pickering, K. E., Stenchikov, G. L. and Ott, L. E.: Lightning-generated NO_x and
20 its impact on tropospheric ozone production: A three-dimensional modeling study of a
21 Stratosphere-Troposphere Experiment: Radiation, Aerosols and Ozone (STERAO-A)
22 thunderstorm, *J. Geophys. Res. D Atmos.*, doi:10.1029/2004JD005556, 2005.
23
24 Dentener, F. J. and Crutzen, P. J.: Reaction of N₂O₅ on tropospheric aerosols: impact on the
25 global distributions of NO_x, O₃, and OH, *J. Geophys. Res.*, doi:10.1029/92JD02979, 1993.
26
27 Dignon, J. and Hameed, S.: Global emissions of nitrogen and sulfur oxides from 1860 to 1980, *J.*
28 *Air Waste Manag. Assoc.*, doi:10.1080/08940630.1989.10466519, 1989.
29
30 Dreher, D. B. and Harley, R. A.: A fuel-based inventory for heavy-duty diesel truck emissions, *J.*
31 *Air Waste Manag. Assoc.*, doi:10.1080/10473289.1998.10463686, 1998.
32
33 Duncan, B. N., Yoshida, Y., De Foy, B., Lamsal, L. N., Streets, D. G., Lu, Z., Pickering, K. E.
34 and Krotkov, N. A.: The observed response of Ozone Monitoring Instrument (OMI) NO₂
35 columns to NO_x emission controls on power plants in the United States: 2005-2011, *Atmos.*
36 *Environ.*, doi:10.1016/j.atmosenv.2013.08.068, 2013.
37
38 Elliott, E. M., Kendall, C., Boyer, E. W., Burns, D. A., Lear, G. G., Golden, H. E., Harlin, K.,
39 Bytnerowicz, A., Butler, T. J. and Glatz, R.: Dual nitrate isotopes in dry deposition: Utility for
40 partitioning NO_x source contributions to landscape nitrogen deposition, *J. Geophys. Res.*
41 *Biogeosciences*, doi:10.1029/2008JG000889, 2009.
42
43 Elliott, E. M., Kendall, C., Wankel, S. D., Burns, D. A., Boyer, E. W., Harlin, K., Bain, D. J. and
44 Butler, T. J.: Nitrogen isotopes as indicators of NO_x source contributions to atmospheric nitrate
45 deposition across the midwestern and northeastern United States, *Environ. Sci. Technol.*,
46 doi:10.1021/es070898t, 2007.

1
2 Farrell, A., Carter, R. and Raufer, R.: The NO_x Budget: Market-based control of tropospheric
3 ozone in the northeastern United States, *Resour. Energy Econ.*, doi:10.1016/S0928-
4 7655(98)00035-9, 1999.
5
6 Fehr, T., Höller, H. and Huntreiser, H.: Model study on production and transport of lightning-
7 produced NO_x in a EULINOX supercell storm, *J. Geophys. Res. D Atmos.*,
8 doi:10.1029/2003JD003935, 2004.
9
10 Felix, J. D., Elliott, E. M. and Shaw, S. L.: Nitrogen isotopic composition of coal-fired power
11 plant NO_x: Influence of emission controls and implications for global emission inventories,
12 *Environ. Sci. Technol.*, doi:10.1021/es203355v, 2012.
13
14 Felix, J. D. and Elliott, E. M.: The agricultural history of human-nitrogen interactions as
15 recorded in ice core δ¹⁵N-NO₃⁻, *Geophys. Res. Lett.*, doi:10.1002/grl.50209, 2013.
16
17 Felix, J. D. and Elliott, E. M.: Isotopic composition of passively collected nitrogen dioxide
18 emissions: Vehicle, soil and livestock source signatures, *Atmos. Environ.*,
19 doi:10.1016/j.atmosenv.2014.04.005, 2014.
20
21 Felix, J. D., Elliott, E. M., Avery, G. B., Kieber, R. J., Mead, R. N., Willey, J. D. and Mullaugh,
22 K. M.: Isotopic composition of nitrate in sequential Hurricane Irene precipitation samples:
23 Implications for changing NO_x sources, *Atmos. Environ.*, doi:10.1016/j.atmosenv.2015.01.075,
24 2015.
25
26 Fang, H., Walters, W. W., Mase, D., and Michalski, G.: i_NRACM: incorporating ¹⁵N into the
27 Regional Atmospheric Chemistry Mechanism (RACM) for assessing the role photochemistry
28 plays in controlling the isotopic composition of NO_x, NO_y, and atmospheric nitrate, *Geosci.*
29 *Model Dev.*, 14, 5001–5022, <https://doi.org/10.5194/gmd-14-5001-2021>, 2021.
30
31 Fibiger, D. L., Hastings, M. G., Lew, A. F. and Peltier, R. E.: Collection of NO and NO₂ for
32 isotopic analysis of NO_x emissions, *Anal. Chem.*, doi:10.1021/ac502968e, 2014.
33
34 Fraser, A., Goutail, F., McLinden, C. A., Melo, S. M. L. and Strong, K.: Lightning-produced
35 NO₂ observed by two ground-based UV-visible spectrometers at Vanscoy, Saskatchewan in
36 August 2004, *Atmos. Chem. Phys.*, doi:10.5194/acp-7-1683-2007, 2007.
37
38 Fujita, E. M., Croes, B. E., Bennett, C. L., Lawson, D. R., Lurmann, F. W. and Main, H. H.:
39 Comparison of emission inventory and ambient concentration ratios of CO, NMOG, and NO_x in
40 California's South Coast Air Basin, *J. Air Waste Manag. Assoc.*,
41 doi:10.1080/10473289.1992.10466989, 1992.
42
43 Fujita, E. M., Campbell, D. E., Zielinska, B. B., Sagebiel, J. C., Bowen, J. L., Goliff, W. S.,
44 Stockwell, W. R. and Lawson, D. R.: Diurnal and weekday variations in the source contributions
45 of ozone precursors in California's South Coast Air Basin, *J. Air Waste Manag. Assoc.*,
46 doi:10.1080/10473289.2003.10466226, 2003.

1
2 Fujita, E. M., Stockwell, W. R., Campbell, D. E., Keislar, R. E. and Lawson, D. R.: Evolution of
3 the magnitude and spatial extent of the weekend ozone effect in California's South Coast Air
4 Basin, 1981–2000, *J. Air Waste Manag. Assoc.*, doi:10.1080/10473289.2003.10466225, 2003.
5
6 Galbally, I. E. and Roy, C. R.: Loss of fixed nitrogen from soils by nitric oxide exhalation,
7 *Nature*, doi:10.1038/275734a0, 1978
8
9 Gallardo, L. and Rodhe, H.: Oxidized nitrogen in the remote Pacific: The role of electrical
10 discharges over the oceans, *J. Atmos. Chem.*, doi:10.1023/A:1005738402496, 1997.
11
12 Galloway, J. N. and Cowling, E. B.: Reactive nitrogen and the world: 200 Years of change, in
13 *Ambio*, 2002.
14
15 Galloway, J. N., Dentener, F. J., Capone, D. G., Boyer, E. W., Howarth, R. W., Seitzinger, S. P.,
16 Asner, G. P., Cleveland, C. C., Green, P. A., Holland, E. A., Karl, D. M., Michaels, A. F., Porter,
17 J. H., Townsend, A. R. and Vörösmarty, C. J.: Nitrogen cycles: Past, present, and future,
18 *Biogeochemistry*, doi:10.1007/s10533-004-0370-0, 2004.
19
20 Ganzeveld, L. N., Lelieveld, J., Dentener, F. J., Krol, M. C., Bouwman, A. J. and Roelofs, G. J.:
21 Global soil-biogenic NO_x emissions and the role of canopy processes, *J. Geophys. Res. Atmos.*,
22 doi:10.1029/2001JD001289, 2002.
23
24 Garten, C. T.: Nitrogen isotope composition of ammonium and nitrate in bulk precipitation and
25 forest throughfall, *Int. J. Environ. Anal. Chem.*, doi:10.1080/03067319208027017, 1992.
26
27 Gauss, M., Myhre, G., Isaksen, I. S. A., Grewe, V., Pitari, G., Wild, O., Collins, W. J., Dentener,
28 F. J., Ellingsen, K., Gohar, L. K., Hauglustaine, D. A., Iachetti, D., Lamarque, J. F., Mancini, E.,
29 Mickley, L. J., Prather, M. J., Pyle, J. A., Sanderson, M. G., Shine, K. P., Stevenson, D. S., Sudo,
30 K., Szopa, S. and Zeng, G.: Radiative forcing since preindustrial times due to ozone change in
31 the troposphere and the lower stratosphere, *Atmos. Chem. Phys.*, doi:10.5194/acp-6-575-2006,
32 2006.
33
34 Grell, G. A., Dudhia, J., & Stauffer, D. R.: A description of the fifth-generation Penn State/NCAR
35 mesoscale model (MM5), NCAR Technical Note NCAR/TN-398+ STR, 1994.
36
37 Hall, S. J., Ogata, E. M., Weintraub, S. R., Baker, M. A., Ehleringer, J. R., Czimczik, C. I. and
38 Bowling, D. R.: Convergence in nitrogen deposition and cryptic isotopic variation across urban
39 and agricultural valleys in northern Utah, *J. Geophys. Res. Biogeosciences*,
40 doi:10.1002/2016JG003354, 2016.
41
42 Hanson, P. J. and Lindberg, S. E.: Dry deposition of reactive nitrogen compounds: A review of
43 leaf, canopy and non-foliar measurements, *Atmos. Environ. Part A, Gen. Top.*,
44 doi:10.1016/0960-1686(91)90020-8, 1991.
45

1 Harley, R. A., McKeen, S. A., Pearson, J., Rodgers, M. O. and Lonneman, W. A.: Analysis of
2 motor vehicle emissions during the Nashville/Middle Tennessee Ozone Study, *J. Geophys. Res.*
3 *Atmos.*, doi:10.1029/2000JD900677, 2001.
4
5 Heaton, T. H. E.: $^{15}\text{N}/^{14}\text{N}$ ratios of nitrate and ammonium in rain at Pretoria, South Africa,
6 *Atmos. Environ.*, doi:10.1016/0004-6981(87)90080-1, 1987.
7
8 Heaton, T. H. E.: $^{15}\text{N}/^{14}\text{N}$ ratios of NO_x from vehicle engines and coal-fired power stations,
9 *Tellus B*, doi:10.1034/j.1600-0889.1990.00007.x-i1, 1990.
10
11 Hoering, T.: The isotopic composition of the ammonia and the nitrate ion in rain, *Geochim.*
12 *Cosmochim. Acta*, doi:10.1016/0016-7037(57)90021-2, 1957.
13
14 Houlton, B. Z., Boyer, E., Finzi, A., Galloway, J., Leach, A., Liptzin, D., Melillo, J., Rosenstock,
15 T. S., Sobota, D. and Townsend, A. R.: Intentional versus unintentional nitrogen use in the
16 United States: Trends, efficiency and implications, *Biogeochemistry*, doi:10.1007/s10533-012-
17 9801-5, 2013.
18
19 Houyoux, M.: Clean Air Interstate Rule Emissions Inventory Technical Support Document. US
20 EPA, 2005.
21
22 Hudman, R. C., Moore, N. E., Mebust, A. K., Martin, R. V., Russell, A. R., Valin, L. C. and
23 Cohen, R. C.: Steps towards a mechanistic model of global soil nitric oxide emissions:
24 Implementation and space based-constraints, *Atmos. Chem. Phys.*, doi:10.5194/acp-12-7779-
25 2012, 2012.
26
27 Huntrieser, H., Schlager, H., Feigl, C. and Höller, H.: Transport and production of NO_x in
28 electrified thunderstorms: Survey of previous studies and new observations at midlatitudes, *J.*
29 *Geophys. Res. Atmos.*, doi:10.1029/98JD02353, 1998.
30
31 Huntrieser, H., Feigl, C., Schlager, H., Schröder, F., Gerbig, C., van Velthoven, P., Flatøy, F.,
32 Théry, C., Petzold, A., Höller, H. and Schumann, U.: Airborne measurements of NO_x , tracer
33 species, and small particles during the European lightning nitrogen oxides experiment, *J.*
34 *Geophys. Res. Atmos.*, doi:10.1029/2000jd000209, 2002.
35
36 Ingalls, M. N.: On-road vehicle emission factors from measurements in a Los Angeles area
37 tunnel, in *Proceedings - A&WMA Annual Meeting.*, 1989.
38
39 Jacob, D. J. and Wofsy, S. C.: Budgets of reactive nitrogen, hydrocarbons, and ozone over the
40 Amazon forest during the wet season, *J. Geophys. Res.*, doi:10.1029/jd095id10p16737, 1990.
41
42 Jaeglé, L., Steinberger, L., Martin, R. V. and Chance, K.: Global partitioning of NO_x sources
43 using satellite observations: Relative roles of fossil fuel combustion, biomass burning and soil
44 emissions, in *Faraday Discussions.*, 2005.
45

1 Johansson, C.: Pine forest: a negligible sink for atmospheric NO_x in rural Sweden, *Tellus B*
2 *Chem. Phys. Meteorol.*, doi:10.3402/tellusb.v39i5.15360, 1987.
3
4 Kim, S. W., Heckel, A., Frost, G. J., Richter, A., Gleason, J., Burrows, J. P., McKeen, S., Hsie,
5 E. Y., Granier, C. and Trainer, M.: NO₂ columns in the western United States observed from
6 space and simulated by a regional chemistry model and their implications for NO_x emissions, *J.*
7 *Geophys. Res. Atmos.*, doi:10.1029/2008JD011343, 2009.
8
9 Koike, M., Kondo, Y., Kita, K., Takegawa, N., Nishi, N., Kashihara, T., Kawakami, S., Kudoh,
10 S., Blake, D., Shirai, T., Liley, B., Ko, M. K., Miyazaki, Y., Kawasaki, Z. and Ogawa, T.:
11 Measurements of reactive nitrogen produced by tropical thunderstorms during BIBLE-C, *J.*
12 *Geophys. Res. Atmos.*, doi:10.1029/2006JD008193, 2007.
13
14 Laughner, J. L., & Cohen, R. C.: Direct observation of changing NO_x lifetime in North
15 American cities, *Science*, 366(6466), 723-727, 2019.
16
17 Lawrence, M. G., Chameides, W. L., Kasibhatla, P. S., Levy, H. and Moxim, W.: Lightning and
18 atmospheric chemistry: The rate of atmospheric NO production, in *Handbook of Atmospheric*
19 *Electrodynamics.*, 2017.
20
21 Lerda, M. T., Munger, J. W. and Jacob, D. J.: The NO₂ flux conundrum, *Science* (80-.),
22 doi:10.1126/science.289.5488.2291, 2000.
23
24 Levy, H., Moxim, W. J. and Kasibhatla, P. S.: A global three-dimensional time-dependent
25 lightning source of tropospheric NO_x, *J. Geophys. Res. Atmos.*, doi:10.1029/96jd02341, 1996.
26
27 Li, D. and Wang, X.: Nitrogen isotopic signature of soil-released nitric oxide (NO) after fertilizer
28 application, *Atmos. Environ.*, doi:10.1016/j.atmosenv.2008.01.042, 2008.
29
30 Li, Y., Schichtel, B. A., Walker, J. T., Schwede, D. B., Chen, X., Lehmann, C. M. B., Puchalski,
31 M. A., Gay, D. A. and Collett, J. L.: Increasing importance of deposition of reduced nitrogen in
32 the United States, *Proc. Natl. Acad. Sci. U. S. A.*, doi:10.1073/pnas.1525736113, 2016.
33
34 Liao, T., Gui, K., Jiang, W., Wang, S., Wang, B., Zeng, Z., Che, H., Wang, Y. and Sun, Y.: Air
35 stagnation and its impact on air quality during winter in Sichuan and Chongqing, southwestern
36 China, *Sci. Total Environ.*, doi:10.1016/j.scitotenv.2018.04.122, 2018.
37
38 Lighty, J. A. S., Veranth, J. M. and Sarofim, A. F.: Combustion aerosols: Factors governing their
39 size and composition and implications to human health, *J. Air Waste Manag. Assoc.*,
40 doi:10.1080/10473289.2000.10464197, 2000.
41
42 Liu, L., Guo, J., Miao, Y., Liu, L., Li, J., Chen, D., He, J. and Cui, C.: Elucidating the
43 relationship between aerosol concentration and summertime boundary layer structure in central
44 China, *Environ. Pollut.*, doi:10.1016/j.envpol.2018.06.008, 2018.
45

1 Lu, Z., Streets, D. G., De Foy, B., Lamsal, L. N., Duncan, B. N. and Xing, J.: Emissions of
2 nitrogen oxides from US urban areas: Estimation from Ozone Monitoring Instrument retrievals
3 for 2005-2014, *Atmos. Chem. Phys.*, doi:10.5194/acp-15-10367-2015, 2015.
4
5 Ludwig, J., Meixner, F. X., Vogel, B. and Forstner, J.: Soil-air exchange of nitric oxide: An
6 overview of processes, environmental factors, and modeling studies, *Biogeochemistry*,
7 doi:10.1023/A:1006424330555, 2001.
8
9 Martin, R. V., Sauvage, B., Folkins, I., Sioris, C. E., Booone, C., Bernath, P. and Ziemke, J.:
10 Space-based constraints on the production of nitric oxide by lightning, *J. Geophys. Res. Atmos.*,
11 doi:10.1029/2006JD007831, 2007.
12
13 Mase, D. F.: A coupled modeling and observational approach to understanding oxygen-18 in
14 atmospheric nitrate, Ph. D. thesis, Purdue University, United States of America, 2010.
15
16 McDonald, B. C., McKeen, S. A., Cui, Y. Y., Ahmadov, R., Kim, S. W., Frost, G. J., ... &
17 Trainer, M.: Modeling ozone in the eastern US using a fuel-based mobile source emissions
18 inventory, *Environmental science & technology*, 52(13), 7360-7370, 2018.
19
20 Miao, Y., Guo, J., Liu, S., Zhao, C., Li, X., Zhang, G., Wei, W. and Ma, Y.: Impacts of synoptic
21 condition and planetary boundary layer structure on the trans-boundary aerosol transport from
22 Beijing-Tianjin-Hebei region to northeast China, *Atmos. Environ.*,
23 doi:10.1016/j.atmosenv.2018.03.005, 2018.
24
25 Miao, Y., Li, J., Miao, S., Che, H., Wang, Y., Zhang, X., Zhu, R. and Liu, S.: Interaction
26 Between Planetary Boundary Layer and PM_{2.5} Pollution in Megacities in China: a Review,
27 *Curr. Pollut. Reports*, doi:10.1007/s40726-019-00124-5, 2019.
28
29 Miller, D. J., Wojtal, P. K., Clark, S. C. and Hastings, M. G.: Vehicle NO_x emission plume
30 isotopic signatures: Spatial variability across the eastern United States, *J. Geophys. Res.*,
31 doi:10.1002/2016JD025877, 2017.
32
33 Miller, D. J., Chai, J., Guo, F., Dell, C. J., Karsten, H. and Hastings, M. G.: Isotopic Composition
34 of In Situ Soil NO_x Emissions in Manure-Fertilized Cropland, *Geophys. Res. Lett.*,
35 doi:10.1029/2018GL079619, 2018.
36
37 Miyazaki, K., Eskes, H. J., & Sudo, K.: Global NO_x emission estimates derived from an
38 assimilation of OMI tropospheric NO₂ columns, *Atmospheric Chemistry and Physics*, 12(5),
39 2263-2288, 2012.
40
41 Moore, H.: The isotopic composition of ammonia, nitrogen dioxide and nitrate in the
42 atmosphere, *Atmos. Environ.*, doi:10.1016/0004-6981(77)90102-0, 1977.
43
44 Muller, J. F.: Geographical distribution and seasonal variation of surface emissions and
45 deposition velocities of atmospheric trace gases, *J. Geophys. Res.*, doi:10.1029/91JD02757,
46 1992.

1
2 Müller, J.-F. and Stavrou, T.: Inversion of CO and NO_x emissions using the adjoint of the
3 IMAGES model, *Atmos. Chem. Phys.*, doi:10.5194/acp-5-1157-2005, 2005.
4
5 Murray, L. T.: Lightning NO_x and Impacts on Air Quality, *Curr. Pollut. Reports*,
6 doi:10.1007/s40726-016-0031-7, 2016.
7
8 National Centers for Environmental Information: U.S. Wind Climatology, Available from:
9 <https://www.ncdc.noaa.gov/societal-impacts/wind/>, 2019.
10
11 National Centers for Environmental Information: Model Datasets, available from:
12 <https://www.ncdc.noaa.gov/data-access/model-data/model-datasets>, 2019.
13
14 Occhipinti, C., Aneja, V. P., Showers, W. and Niyogi, D.: Back-trajectory analysis and source-
15 receptor relationships: Particulate matter and nitrogen isotopic composition in rainwater,
16 *Journal of the Air and Waste Management Association.*, 2008.
17
18 Oke, T. R.: *Boundary Layer Climates.*, 2002.
19
20 Ott, L. E., Pickering, K. E., Stenchikov, G. L., Huntrieser, H. and Schumann, U.: Effects of
21 lightning NO_x production during the 21 July European Lightning Nitrogen Oxides Project storm
22 studied with a three-dimensional cloud-scale chemical transport model, *J. Geophys. Res. Atmos.*,
23 doi:10.1029/2006JD007365, 2007.
24
25 Parrish, D. D.: Critical evaluation of US on-road vehicle emission inventories, *Atmos. Environ.*,
26 doi:10.1016/j.atmosenv.2005.11.033, 2006.
27
28 Pearson, J., Wells, D. M., Seller, K. J., Bennett, A., Soares, A., Woodall, J. and Ingrouille, M. J.:
29 Traffic exposure increases natural ¹⁵N and heavy metal concentrations in mosses, *New Phytol.*,
30 doi:10.1046/j.1469-8137.2000.00702.x, 2000.
31
32 Pierce, T. E.: Reconsideration of the Emission Factors assumed in BEIS3 for Three USGS
33 Vegetation Categories: Shrubland, Coniferous Forest, and Deciduous Forest, 2001.
34
35 Pierson, W. R., Gertler, A. W. and Bradow, R. L.: Comparison of the scaqs tunnel study with
36 other onroad vehicle emission data, *J. Air Waste Manag. Assoc.*,
37 doi:10.1080/10473289.1990.10466799, 1990.
38
39 Pierson, W. R., Gertler, A. W., Robinson, N. F., Sagebiel, J. C., Zielinska, B., Bishop, G. A.,
40 Stedman, D. H., Zweidinger, R. B. and Ray, W. D.: Real-world automotive emissions - summary
41 of studies in the Fort McHenry and Tuscarora Mountain Tunnels, in *Atmospheric Environment.*,
42 1996.
43
44 Pilegaard, K.: Processes regulating nitric oxide emissions from soils, *Philos. Trans. R. Soc. B*
45 *Biol. Sci.*, doi:10.1098/rstb.2013.0126, 2013.
46

1 Potter, C. S., Matson, P. A., Vitousek, P. M. and Davidson, E. A.: Process modeling of controls
2 on nitrogen trace gas emissions from soils worldwide, *J. Geophys. Res. Atmos.*,
3 doi:10.1029/95JD02028, 1996.
4

5 Pouliot, G., & Pierce, T. E.: Integration of the Model of Emissions of Gases and Aerosols from
6 Nature (MEGAN) into the CMAQ Modeling System, in: 18th International Emission Inventory
7 Conference, Baltimore, Maryland, 14 April 2009, 14-17, 2009.
8

9 Rasool, Q. Z., Zhang, R., Lash, B., Cohan, D. S., Cooter, E. J., Bash, J. O., & Lamsal, L. N.:
10 Enhanced representation of soil NO emissions in the Community Multiscale Air Quality (CMAQ)
11 model version 5.0. 2, *Geoscientific Model Development*, 9(9), 3177-3197, 2016
12

13 Redling, K., Elliott, E., Bain, D. and Sherwell, J.: Highway contributions to reactive nitrogen
14 deposition: Tracing the fate of vehicular NO_x using stable isotopes and plant biomonitors,
15 *Biogeochemistry*, doi:10.1007/s10533-013-9857-x, 2013.
16

17 Ridley, B. A., Dye, J. E., Walega, J. G., Zheng, J., Grahek, F. E. and Rison, W.: On the
18 production of active nitrogen by thunderstorms over New Mexico, *J. Geophys. Res. Atmos.*,
19 doi:10.1029/96jd01706, 1996.
20

21 Ridley, B., Ott, L., Pickering, K., Emmons, L., Montzka, D., Weinheimer, A., Knapp, D.,
22 Grahek, F., Li, L., Heymsfield, G., McGill, M., Kucera, P., Mahoney, M. J., Baumgardner, D.,
23 Schultz, M. and Brasseur, G.: Florida thunderstorms: A faucet of reactive nitrogen to the upper
24 troposphere, *J. Geophys. Res. D Atmos.*, doi:10.1029/2004JD004769, 2004.
25

26 Riha, K. M.: The use of stable isotopes to constrain the nitrogen cycle, Ph. D. thesis, Purdue
27 University, United States of America, 2013.
28

29 Russell, K. M., Galloway, J. N., MacKo, S. A., Moody, J. L. and Scudlark, J. R.: Sources of
30 nitrogen in wet deposition to the Chesapeake Bay region, *Atmos. Environ.*, doi:10.1016/S1352-
31 2310(98)00044-2, 1998.
32

33 Savard, M. M., Bégin, C., Smirnoff, A., Marion, J. and Rioux-Paquette, E.: Tree-ring nitrogen
34 isotopes reflect anthropogenic NO_x emissions and climatic effects, *Environ. Sci. Technol.*,
35 doi:10.1021/es802437k, 2009.
36

37 Savard, M. M., Cole, A., Smirnoff, A. and Vet, R.: $\Delta^{15}\text{N}$ values of atmospheric N species
38 simultaneously collected using sector-based samplers distant from sources – Isotopic inheritance
39 and fractionation, *Atmos. Environ.*, doi:10.1016/j.atmosenv.2017.05.010, 2017.
40

41 Sawyer, R. F., Harley, R. A., Cadle, S. H., Norbeck, J. M., Slott, R. and Bravo, H. A.: Mobile
42 sources critical review: 1998 NARSTO assessment, *Atmos. Environ.*, doi:10.1016/S1352-
43 2310(99)00463-X, 2000.
44

1 Scholes, M. C., Martin, R., Scholes, R. J., Parsons, D. and Winstead, E.: NO and N₂O emissions
2 from savanna soils following the first simulated rains of the season, *Nutr. Cycl. Agroecosystems*,
3 doi:10.1023/a:1009781420199, 1997.
4

5 Schumann, U., Kurz, C., Schlager, H., Huntrieser, H., Emmons, L., Labrador, L., Meijer, E.,
6 Ulanovsky, A. and Viciani, S.: Towards a robust estimate of the global lightning nitrogen oxides
7 source rate and its error bound, in European Space Agency, (Special Publication) ESA SP., 2006.
8

9 Schumann, U. and Huntrieser, H.: The global lightning-induced nitrogen oxides source, *Atmos.*
10 *Chem. Phys.*, doi:10.5194/acp-7-3823-2007, 2007.
11

12 Schwartz, S. E.: The Whitehouse effect - Shortwave radiative forcing of climate by
13 anthropogenic aerosols: An overview, *J. Aerosol Sci.*, doi:10.1016/0021-8502(95)00533-1, 1996.
14

15 Schwede, D., Pouliot, G. and Pierce, T.: Changes to the biogenic emissions inventory system
16 version 3 (BEIS3), in 4th Annual CMAS User's Conference., 2005.
17

18 Selden, T. M., Forrest, A. S., & Lockhart, J. E.: Analyzing the reductions in US air pollution
19 emissions: 1970 to 1990, *Land Economics*, 1-21, doi: 10.2307/3146990, 1999.
20

21 Shepherd, M. F., Barzetti, S. and Hastie, D. R.: The production of atmospheric NO_x and N₂O from
22 a fertilized agricultural soil, *Atmos. Environ. Part A, Gen. Top.*, doi:10.1016/0960-
23 1686(91)90277-E, 1991.
24

25 Shu, L., Xie, M., Gao, D., Wang, T., Fang, D., Liu, Q., Huang, A. and Peng, L.: Regional severe
26 particle pollution and its association with synoptic weather patterns in the Yangtze River Delta
27 region, China, *Atmos. Chem. Phys.*, doi:10.5194/acp-17-12871-2017, 2017.
28

29 Singer, B. C. and Harley, R. A.: A Fuel-Based Motor Vehicle Emission Inventory, *J. Air Waste*
30 *Manag. Assoc.*, doi:10.1080/10473289.1996.10467492, 1996.
31

32 Singer, B. C. and Harley, R. A.: A fuel-based inventory of motor vehicle exhaust emissions in the
33 Los Angeles area during summer 1997, *Atmos. Environ.*, doi:10.1016/S1352-2310(99)00358-1,
34 2000.
35

36 Skamarock, W. C., Dye, J. E., Defer, E., Barth, M. C., Stith, J. L., Ridley, B. A. and Baumann, K.:
37 Observational- and modeling-based budget of lightning-produced NO_x in a continental
38 thunderstorm, *J. Geophys. Res. Atmos.*, doi:10.1029/2002jd002163, 2003.
39

40 Slovik, S., Siegmund, A., Fuhrer, H. W. and Heber, U.: Stomatal uptake of SO₂, NO_x and O₃ by
41 spruce crowns (*Picea abies*) and canopy damage in Central Europe, *New Phytol.*,
42 doi:10.1111/j.1469-8137.1996.tb01884.x, 1996.
43

44 Snape, C. E., Sun, C., Fallick, A. E., Irons, R. and Haskell, J.: Potential of stable nitrogen isotope
45 ratio measurements to resolve fuel and thermal NO_x in coal combustion, *Fuel Chem. Div. Prepr.*,
46 2003.

1
2 Snyder, J. P.: Map projections - a working manual, US Geol. Surv. Prof. Pap., 1987.
3
4 Song, W., Liu, X. Y., Hu, C. C., Chen, G. Y., Liu, X. J., Walters, W. W., ... & Liu, C. Q.:
5 Important contributions of non-fossil fuel nitrogen oxides emissions, Nature communications,
6 12(1), 1-7, 2021
7
8 Spak, S., Holloway, T., Mednick, A., & Stone, B.: Evaluation of Bottom-Up Mobile Emissions
9 Inventories in the Upper Midwest, in: American Geophysical Union Fall Meeting, San Francisco,
10 California, 10-14 Dec 2007, 2007.
11
12 Srivastava, R. K., Neuffer, W., Grano, D., Khan, S., Staudt, J. E. and Jozewicz, W.: Controlling
13 NO_x emission from industrial sources, Environ. Prog., doi:10.1002/ep.10063, 2005.
14
15 Staudt, A. C., Jacob, D. J., Ravetta, F., Logan, J. A., Bachiochi, D., Sandholm, S., Ridley, B.,
16 Singh, H. B. and Talbot, B.: Sources and chemistry of nitrogen oxides over the tropical Pacific,
17 J. Geophys. Res. Atmos., doi:10.1029/2002jd002139, 2003.
18
19 Stavrou, T., Müller, J. F., Boersma, K. F., Van Der A., R. J., Kurokawa, J., Ohara, T. and
20 Zhang, Q.: Key chemical NO_x sink uncertainties and how they influence top-down emissions of
21 nitrogen oxides, Atmos. Chem. Phys., doi:10.5194/acp-13-9057-2013, 2013.
22
23 Stehfest, E. and Bouwman, L.: N₂O and NO emission from agricultural fields and soils under
24 natural vegetation: Summarizing available measurement data and modeling of global annual
25 emissions, Nutr. Cycl. Agroecosystems, doi:10.1007/s10705-006-9000-7, 2006.
26
27 Stevenson, D. S., Dentener, F. J., Schultz, M. G., Ellingsen, K., van Noije, T. P. C., Wild, O.,
28 Zeng, G., Amann, M., Atherton, C. S., Bell, N., Bergmann, D. J., Bey, I., Butler, T., Cofala, J.,
29 Collins, W. J., Derwent, R. G., Doherty, R. M., Drevet, J., Eskes, H. J., Fiore, A. M., Gauss, M.,
30 Hauglustaine, D. A., Horowitz, L. W., Isaksen, I. S. A., Krol, M. C., Lamarque, J. F., Lawrence,
31 M. G., Montanaro, V., Müller, J. F., Pitari, G., Prather, M. J., Pyle, J. A., Rast, S., Rodriguez, J.
32 M., Sanderson, M. G., Savage, N. H., Shindell, D. T., Strahan, S. E., Sudo, K. and Szopa, S.:
33 Multimodel ensemble simulations of present-day and near-future tropospheric ozone, J.
34 Geophys. Res. Atmos., doi:10.1029/2005JD006338, 2006.
35
36 The Institute for the Environment - The University of North Carolina at Chapel Hill: SMOKE v4.5
37 User's Manual, Available from: <https://www.cmascenter.org/smoke/documentation/4.5/html/>,
38 2017.
39
40 Thoene, B., Rennenberg, H. and Weber, P.: Absorption of atmospheric NO₂ by spruce (*Picea*
41 *abies*) trees: II. Parameterization of NO₂ fluxes by controlled dynamic chamber experiments,
42 New Phytol., doi:10.1111/j.1469-8137.1996.tb04630.x, 1996.
43
44 Thomas, R. J., Krehbiel, P. R., Rison, W., Hamlin, T., Boccippio, D. J., Goodman, S. J. and
45 Christian, H. J.: Comparison of ground-based 3-dimensional lightning mapping observations

1 with satellite-based LIS observations in Oklahoma, *Geophys. Res. Lett.*,
2 doi:10.1029/1999GL010845, 2000.
3
4 Tie, X., Zhang, R., Brasseur, G. and Lei, W.: Global NO_x production by lightning, *J. Atmos.*
5 *Chem.*, doi:10.1023/A:1016145719608, 2002.
6
7 Tost, H., Jöckel, P. and Lelieveld, J.: Lightning and convection parameterisations - Uncertainties
8 in global modelling, *Atmos. Chem. Phys.*, doi:10.5194/acp-7-4553-2007, 2007.
9
10 United States Census Bureau: 2007–2011 American Community Survey 5-Year Estimates, travel
11 time to work by zip code, table B08303, Available from: [https://www.census.gov/programs-](https://www.census.gov/programs-surveys/acs/technical-documentation/table-and-geography-changes/2011/5-year.html)
12 [surveys/acs/technical-documentation/table-and-geography-changes/2011/5-year.html](https://www.census.gov/programs-surveys/acs/technical-documentation/table-and-geography-changes/2011/5-year.html), 2019.
13
14 United States Energy Information Administration: Electricity, Available from:
15 <https://www.eia.gov/electricity/data/eia860/>, 2017a.
16
17 United States Energy Information Administration: U.S. electric generating capacity increase in
18 2016 was largest net change since 2011, Available from:
19 <https://www.eia.gov/todayinenergy/detail.php?id=30112>, 2017b.
20
21 United States Environmental Protection Agency: National Emissions Inventory (NEI), Available
22 from: <https://www.epa.gov/air-emissions-inventories/national-emissions-inventory-nei>, 2014.
23
24 United States Environmental Protection Agency: Biogenic Emissions Landuse Database,
25 Available from: [https://www.epa.gov/air-emissions-modeling/biogenic-emissions-landuse-](https://www.epa.gov/air-emissions-modeling/biogenic-emissions-landuse-database-version-3-beld3)
26 [database-version-3-beld3](https://www.epa.gov/air-emissions-modeling/biogenic-emissions-landuse-database-version-3-beld3), 2018a.
27
28 United States Environmental Protection Agency: 2002 National Emissions Inventory (NEI)
29 Booklet, Available from: [https://archive.epa.gov/epa/air-emissions-inventories/2002-national-](https://archive.epa.gov/epa/air-emissions-inventories/2002-national-emissions-inventory-nei-booklet.html)
30 [emissions-inventory-nei-booklet.html](https://archive.epa.gov/epa/air-emissions-inventories/2002-national-emissions-inventory-nei-booklet.html), 2018b
31
32 US Environmental Protection Agency: User's Guide to MOBILE6.1 and MOBILE6.2 Mobile
33 Source Emission Factor Model, Tech. Rep. EPA420-R-03-010, 2003.
34
35 Van Noije, T. P. C., Eskes, H. J., Dentener, F. J., Stevenson, D. S., Ellingsen, K., Schultz, M. G.,
36 Wild, O., Amann, M., Atherton, C. S., Bergmann, D. J., Bey, I., Boersma, K. F., Butler, T.,
37 Cofala, J., Drevet, J., Fiore, A. M., Gauss, M., Hauglustaine, D. A., Horowitz, L. W., Isaksen, I.
38 S. A., Krol, M. C., Lamarque, J. F., Lawrence, M. G., Martin, R. V., Montanaro, V., Müller, J.
39 F., Pitari, G., Prather, M. J., Pyle, J. A., Richter, A., Rodriguez, J. M., Savage, N. H., Strahan, S.
40 E., Sudo, K., Szopa, S. and Van Roozendaal, M.: Multi-model ensemble simulations of
41 tropospheric NO₂ compared with GOME retrievals for the year 2000, *Atmos. Chem. Phys.*,
42 doi:10.5194/acp-6-2943-2006, 2006.
43
44 Vinken, G. C. M., Boersma, K. F., Maasakkers, J. D., Adon, M., & Martin, R. V.: Worldwide
45 biogenic soil NO_x emissions inferred from OMI NO₂ observations, *Atmospheric Chemistry*
46 *and Physics*, 14(18), 10363-10381, 2014

1
2 Vukovich, J., & Pierce, T.: The implementation of BEIS3 within the SMOKE modeling framework,
3 in: Proceedings of the 11th International Emissions Inventory Conference, Atlanta, Georgia, 15
4 April 2002, 15-18, 2002.
5
6 Walters, W. W., Goodwin, S. R. and Michalski, G.: Nitrogen stable isotope composition ($\delta^{15}\text{N}$)
7 of vehicle-emitted NO_x, Environ. Sci. Technol., doi:10.1021/es505580v, 2015a.
8
9 Walters, W. W., Tharp, B. D., Fang, H., Kozak, B. J. and Michalski, G.: Nitrogen Isotope
10 Composition of Thermally Produced NO_x from Various Fossil-Fuel Combustion Sources,
11 Environ. Sci. Technol., doi:10.1021/acs.est.5b02769, 2015b.
12
13 Walters, W. W. and Michalski, G.: Theoretical calculation of nitrogen isotope equilibrium
14 exchange fractionation factors for various NO_y molecules, Geochim. Cosmochim. Acta,
15 doi:10.1016/j.gca.2015.05.029, 2015.
16
17 Walters, W. W., Simonini, D. S. and Michalski, G.: Nitrogen isotope exchange between NO and
18 NO₂ and its implications for $\delta^{15}\text{N}$ variations in tropospheric NO_x and atmospheric nitrate,
19 Geophys. Res. Lett., doi:10.1002/2015GL066438, 2016.
20
21 Walters, W. W., Fang, H. and Michalski, G.: Summertime diurnal variations in the isotopic
22 composition of atmospheric nitrogen dioxide at a small midwestern United States city, Atmos.
23 Environ., doi:10.1016/j.atmosenv.2018.01.047, 2018.
24
25 Weber, P. and Rennenberg, H.: Dependency of nitrogen dioxide (NO₂) fluxes to wheat (*Triticum*
26 *aestivum* L.) leaves from NO₂ concentration, light intensity, temperature and relative humidity
27 determined from controlled dynamic chamber experiments, Atmos. Environ., doi:10.1016/1352-
28 2310(96)00008-8, 1996.
29
30 Wong, S., Wang, W. C., Isaksen, I. S. A., Berntsen, T. K. and Sundet, J. K.: A global climate-
31 chemistry model study of present-day tropospheric chemistry and radiative forcing from changes
32 in tropospheric O₃ since the preindustrial period, J. Geophys. Res. D Atmos.,
33 doi:10.1029/2003JD003998, 2004.
34
35 Xing, J., Pleim, J., Mathur, R., Pouliot, G., Hogrefe, C., Gan, C. M. and Wei, C.: Historical
36 gaseous and primary aerosol emissions in the United States from 1990 to 2010, Atmos. Chem.
37 Phys., doi:10.5194/acp-13-7531-2013, 2013.
38
39 Yan, X., Ohara, T. and Akimoto, H.: Statistical modeling of global soil NO_x emissions, Global
40 Biogeochem. Cycles, doi:10.1029/2004GB002276, 2005.
41
42 Yienger, J. J. and Levy, H.: Empirical model of global soil-biogenic NO_x emissions, J. Geophys.
43 Res., doi:10.1029/95jd00370, 1995.
44
45 Yu, Z. and Elliott, E. M.: Novel Method for Nitrogen Isotopic Analysis of Soil-Emitted Nitric
46 Oxide, Environ. Sci. Technol., doi:10.1021/acs.est.7b00592, 2017.

1
2 Zörner, J., Penning de Vries, M. J. M., Beirle, S., Sihler, H., Veres, P. R., Williams, J. and
3 Wagner, T.: Multi-satellite sensor study on precipitation-induced emission pulses of NO_x from
4 soils in semi-arid ecosystems, *Atmos. Chem. Phys. Discuss.*, doi:10.5194/acp-2016-93, 2016.